Supporting Information:

A metal-metal quadruply bonded dimer of two pincer-ligated metal centers

Souvik Mandal,[a] Ethan Y. Song,[a] Thomas J. Emge,[a] Faraj Hasanayn*[b] and Alan S. Goldman*[a]

[a] *Department of Chemistry and Chemical Biology, Rutgers, The State University of New Jersey, New Brunswick, New Jersey 08901, United States*

[b] *Department of Chemistry, American University of Beirut, Beirut 1107 2020, Lebanon*

*Email: fh19@aub.edu.lb; alan.goldman@rutgers.edu

Table of Contents

I. General considerations

Unless otherwise noted all reactions were performed in an argon-filled glove box, or using standard Schlenk techniques. Chemicals were purchased from Sigma Aldrich, Fisher Scientific, or other commercial sources, and used without further purification. Anhydrous reagent-grade solvents were purchased from Sigma-Aldrich and degassed before use by sparging with argon. Deuterated solvents including $CDCl_3$, C_6D_6, toluene-d_8, CD_3CN and THF-d_8 were purchased from Cambridge Isotope Laboratories and deoxygenated with three freeze-pump-thaw cycles, dried over neutral alumina, and stored over molecular sieves prior to use.

$P^{Ar}N(H)P$,[S1] ($P^{Ar}NP$)$MoBr_3$ (**LMoBr$_3$**),[S2] were prepared according to the reported literature processes.

All NMR spectra (^1H (500 MHz), $^{31}P\{^1H\}$ (202 MHz), $^{13}C\{^1H\}$(125.0 MHz) were acquired on a Bruker Avance 500-MHz or Varian VNMRS 500-MHz NMR spectrometer at ambient temperature (25 °C) unless noted otherwise. ^1H NMR chemical shifts are reported relative to TMS and were referenced via residual ^1H resonances of the corresponding deuterated solvent (C_6D_6: δ 7.16 ppm, THF-d_8: δ 3.58, toluene-d_8: δ 2.09, CD_3CN: δ 1.84). $^{31}P\{^1H\}$ NMR signals are given relative to 85% H_3PO_4, $^{13}C\{^1H\}$ NMR chemical shifts are reported relative to TMS.

Evans method measurements of magnetic susceptibility were performed using a sealed capillary containing benzene (50 mM in THF-d_8), while the NMR tube contained 10 mM benzene in the analyte solution (total volume 0.5 mL).[S3,S4]

X-ray crystallographic data were obtained at 100K using a Bruker SMART Apex CCD diffractometer with graphite monochromatized MoKα radiation (λ = 0.71073Å) or a Rigaku XTALab Synergy-S diffractometer (HyPix-6000HE area detector) with monochromatized CuKα radiation (λ = 1.5418Å). Crystals were immersed in Paraffin/Paratone oil (3:1) and placed on a nylon loop. The data were corrected for Lorentz effects, polarization, and absorption, the latter by a multi-scan (SADABS) method[S5]. The structures were solved by direct methods (SHELXS86)[S6] or a dual-space algorithm (SHELXT)[S7]. All non-hydrogen atoms were refined (SHELXL)[S8] based upon F^2_{obs}. All hydrogen atom coordinates were calculated with idealized geometries (SHELXL). Scattering factors (f_o, f', f") are as described in SHELXL. Atomic coordinates, bond angles and torsions can be found with the associated .cif files. ORTEP-like graphics were produced with the XP application in SHELXTL.[S9] Additional software used includes the Cambridge Structural Database[S10] and Mercury[S11] programs from CCDC.

II. Synthesis of molybdenum complexes

S2.1 Synthesis of 1

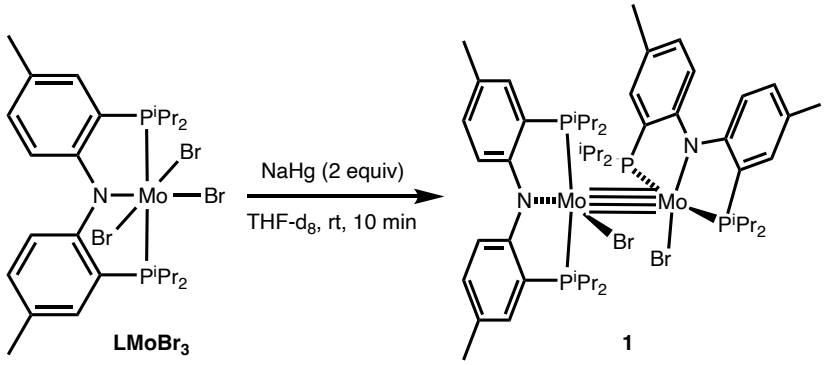

To a J. Young NMR tube, **LMoBr$_3$** (7.6 mg, 0.010 mmol, 1.0 equiv) was weighed and dissolved in 0.5 mL of THF-d_8. To this solution 0.5 w/w% sodium amalgam (Na/Hg) (92.0 mg, 0.020 mmol Na, 2.0 equiv) was added and the mixture was shaken vigorously. The solution color changed to purple and metallic mercury settled to the bottom of the NMR tube. The NMR was quickly recorded and the $^{31}P\{^1H\}$ NMR spectrum appeared as an AB doublet at δ 37.0 and δ 29.5 ppm with coupling constant $^2J_{PP}$ = 104 Hz. An X-ray quality crystal of **1** was grown via slow diffusion of pentane to a saturated solution of **1** in THF at -35 °C (S3.1; Figure S1).

^{1}H NMR: (THF-d_8, 500 MHz): δ 7.48 (d, *J* = 5.2 Hz, 4H), 7.19 (dd, *J* = 9.0, 4.1 Hz, 2H), 6.94 (dd, *J* = 12.6, 7.5 Hz, 4H), 6.66 (d, *J* = 8.8 Hz, 2H), 4.70 – 4.60 (m, 2H), 2.87 – 2.81 (m, 2H), 2.30 (s, 6H), 2.25 – 2.21 (m, 2H), 2.08 (s, 6H), 1.92 (dd, *J* = 17.1, 7.4 Hz, 6H), 1.53 – 1.47 (m, 2H), 1.33 (td, *J* = 16.3, 7.6 Hz, 6H), 1.20 (dd, *J* = 11.4, 7.0 Hz, 6H), 1.07 (dd, *J* = 12.9, 7.4 Hz, 6H), 0.89 (t, *J* = 7.0 Hz, 6H), 0.64 (dd, *J* = 11.1, 7.2 Hz, 6H), 0.57 (d, *J* = 10.1 Hz, 6H), 0.49 (dd, *J* = 14.0, 6.9 Hz, 6H).

$^{31}P\{^1H\}$ NMR: (THF-d_8, 202 MHz): δ 37.0 (d, *J* = 104.2 Hz), 29.5 (d, *J* = 104.2 Hz).

$^{13}C\{^1H\}$ NMR: (THF-d_8, 125 MHz): δ 162.3 (d, *J* = 18.7 Hz), 159.1 (d, *J* = 20.8 Hz), 134.6, 133.2, 132.5, 132.3, 130.3, 129.4 (d, *J* = 4.7 Hz), 125.0, 123.1, 118.0 (d, *J* = 27.8 Hz), 116.5 (d, *J* = 2.5 Hz), 35.2, 30.8, 26.6 (d, *J* = 12.0 Hz), 26.5, 23.8, 23.4, 21.3 (d, *J* = 8.4 Hz), 21.1, 20.52, 19.6, 18.4, 17.8, 17.1.

S2.2 Synthesis of LMoBr(THF)$_n$

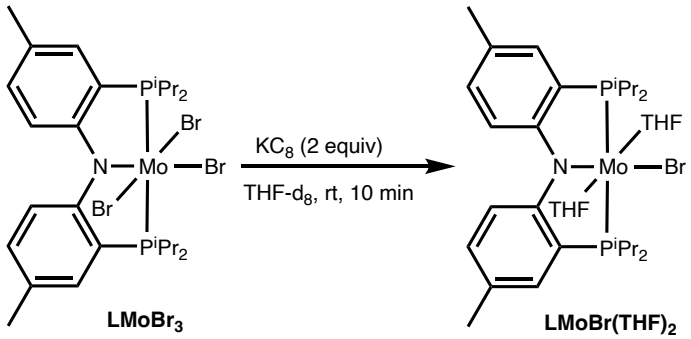

LMoBr$_3$ **LMoBr(THF)$_2$**

Using KC$_8$: To a J. Young NMR tube, **LMoBr$_3$** (7.6 mg, 0.010 mmol, 1.0 equiv) was weighed and dissolved in 0.5 mL of THF-d$_8$. To this solution KC_8 (2.7 mg, 0.020 mmol K, 2.0 equiv) was added and the mixture was shaken (or sonicated). The solution color changed to dark purple, and graphite settled to the bottom of the NMR tube. The NMR was quickly recorded, and no signals were observed in the $^{31}P\{^1H\}$ NMR spectrum; however some signals attributable to paramagnetic species appeared at 72.1 and -28.6 ppm in the ^1H NMR spectrum. This product is assigned as **LMoBr(THF)$_n$**.

^{1}H NMR: (THF-d$_8$, 500 MHz): (all paramagnetic chemical shifts) δ 72.1, 45.4, 23.7, 21.3, 13.5, 11.1, -14.0, -28.6.

Magnetic Susceptibility: Evans Method: 4.6 μ_B

Using Na/Hg: When Na/Hg was added to **LMoBr$_3$**, but without vigorous shaking, the same paramagnetic signals observed in the reaction with KC_8 appeared in the ^1H NMR spectrum, along with signals characteristic of **1**.

Using C$_6$D$_6$ as a solvent: To a J. Young NMR tube, **LMoBr$_3$** (7.6 mg, 0.010 mmol, 1.0 equiv) was weighed and dissolved in 0.5 mL of C_6D_6. To this solution 50 μL of THF-d$_8$ was added, followed by addition of KC_8 (2.7 mg, 0.020 mmol K, 2.0 equiv), and the mixture was shaken (or sonicated). The solution color changed to dark purple, and graphite settled to the bottom of the NMR tube. The NMR spectra were recorded immediately. No signals were observed in the $^{31}P\{^1H\}$ NMR spectrum, and the paramagnetic signals at 72.1, 45.4, and -28.6 ppm (and all others) were observed in the ^1H NMR spectrum, consistent with their attribution to a THF-coordinated Mo(II) paramagnetic species.

S2.3 Further experimental evidence for $LMoBr(THF)_n$

S2.3.1 Reduction of $LMoBr_3$ and trapping of $LMoBr(THF)_n$ with L type ligands

S2.3.1.1 Trapping with CO

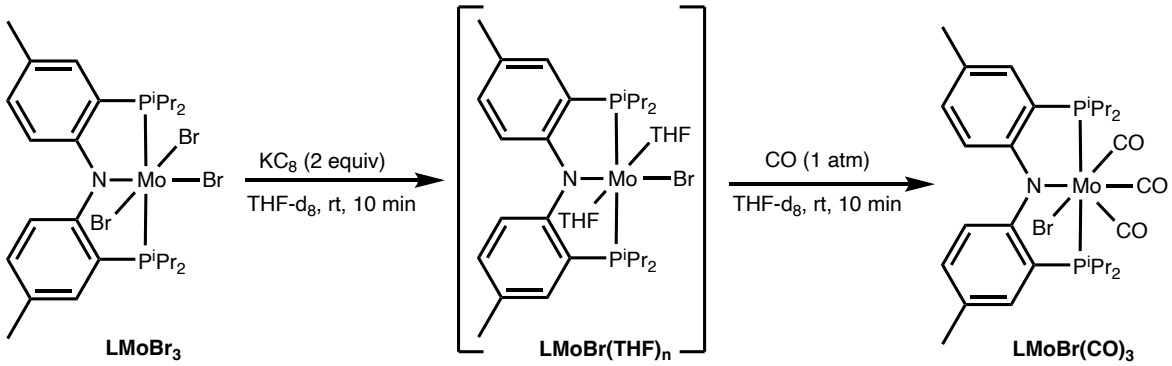

$LMoBr_3$ **$LMoBr(THF)_n$** **$LMoBr(CO)_3$**

To a J. Young NMR tube, **$LMoBr_3$** (7.6 mg, 0.010 mmol, 1.0 equiv) was weighed and dissolved in 0.5 mL of THF-d_8. To this solution KC_8 (2.7 mg, 0.020 mmol K, 2.0 equiv) was added and the mixture was shaken. When the color changed to dark purple, 1 atm CO was charged to the NMR tube and the color changed to red. An AB doublet pattern signal appeared in the $^{31}P\{^1H\}$ NMR spectrum at 57.5 and 53.3 ppm with $^2J_{PP}$ = 167 Hz.

^{1}H NMR: (THF-d_8, 500 MHz): δ 7.20 (d, *J* = 7.5 Hz, 2H), 7.01 (dd, *J* = 8.4, 3.9 Hz, 1H), 6.84 (dd, *J* = 8.4, 3.7 Hz, 2H), 6.73 (d, *J* = 8.3 Hz, 1H), 3.18 (dp, *J* = 11.7, 7.3 Hz, 1H), 3.04 (dp, *J* = 14.0, 7.2 Hz, 1H), 2.74 (septet, *J* = 7.1 Hz, 1H), 2.43 – 2.35 (m, 1H), 2.24 (s, 2H), 2.18 (s, 2H), 1.65 (dd, *J* = 11.7, 7.2 Hz, 3H), 1.55 (dd, *J* = 18.8, 7.4 Hz, 3H), 1.46 (dd, *J* = 15.2, 6.9 Hz, 3H), 1.39 – 1.25 (m, 12H), 1.02 (dd, *J* = 14.4, 6.9 Hz, 3H).

$^{31}P\{^1H\}$ NMR: (THF-d_8, 202 MHz): δ 57.5 (d, *J* = 166.9 Hz), 53.3 (d, *J* = 166.9 Hz).

$^{13}C\{^1H\}$ NMR: (THF-d_8, 125 MHz): δ 247.7 (d, *J* = 8.1 Hz), 227.4 (d, *J* = 24.9 Hz), 222.6 (d, *J* = 18.2 Hz), 164.0 (d, *J* = 17.6 Hz), 159.2 (d, *J* = 18.3 Hz), 133.0 (d, *J* = 2.9 Hz), 131.9 (d, *J* = 2.7 Hz), 130.7 (d, *J* = 11.3 Hz), 127.7 (d, *J* = 7.2 Hz), 127.2 (d, *J* = 7.0 Hz), 119.9 (d, *J* = 9.8 Hz), 118.6 (d, *J* = 9.8 Hz), 35.2, 30.3 (dd, *J* = 15.8, 3.0 Hz), 29.1 (dd, *J* = 12.9, 5.4 Hz), 24.6 (d, *J* = 6.0 Hz), 23.4, 21.6 (d, *J* = 1.7 Hz), 20.8 (d, *J* = 3.3 Hz), 20.6 (d, *J* = 3.9 Hz), 19.9, 19.7 (d, *J* = 4.8 Hz), 19.1 (d, *J* = 2.1 Hz), 18.9 (d, *J* = 2.0 Hz), 18.6 (d, *J* = 3.5 Hz), 14.5.

Trapping with ^{13}CO to yield $LMoBr(^{13}CO)_3$

When ^{13}CO (0.5 atm) was charged to a solution of **$LMoBr(THF)_n$** (in-situ generated via reduction of **$LMoBr_3$**) three distinct ^{13}C NMR signals were observed in the $^{13}C\{^1H\}$ NMR spectrum each showing a total of four couplings (two due to the two other CO ligands, and two due to the two

inequivalent P atoms). Similarly, the $^{31}P\{^{1}H\}$ NMR spectrum revealed that each P signal was further split due to the presence of three inequivalent carbonyls.

$^{31}P\{^{1}H\}$ NMR: (202 MHz, THF-d_8) δ 57.8 (ddt, J = 166.8, 33.5, 5.6 Hz), 53.7 (dddd, J = 166.9, 31.6, 18.6, 8.0 Hz).

$^{13}C\{^{1}H\}$ NMR: (126 MHz, THF-d_8) (only CO region) δ 247.5 (dddd, J = 33.3, 21.7, 14.3, 7.6 Hz), 227.4 (dddd, J = 31.2, 21.5, 6.4, 3.2 Hz), 222.5 (ddt, J = 18.4, 14.1, 4.4 Hz).

LMoI(CO)$_3$: Reduction in the presence of NaI (3 equiv) followed by CO addition leads to formation of **LMoI(CO)$_3$**. The $^{31}P\{^{1}H\}$ NMR spectrum showed a highly roofed AB doublet pattern at 53.5 and 52.4 ppm with $^{2}J_{P\text{-}P}$ = 162 Hz . An X-Ray quality crystal was grown under argon atmosphere via slow diffusion of pentane to a THF solution. A crystal structure (S3.2; **Figure S2**) revealed **LMoI(CO)$_2$** with a distorted octahedral coordination at Mo. This was presumed to be attributable to loss of a CO ligand during recrystallization.

$^{31}P\{^{1}H\}$ NMR: (THF, 202 MHz) δ 53.5 (d, J = 161.6 Hz), 52.4 (d, J = 162.2 Hz).

S2.3.1.2 Trapping with PMe$_3$

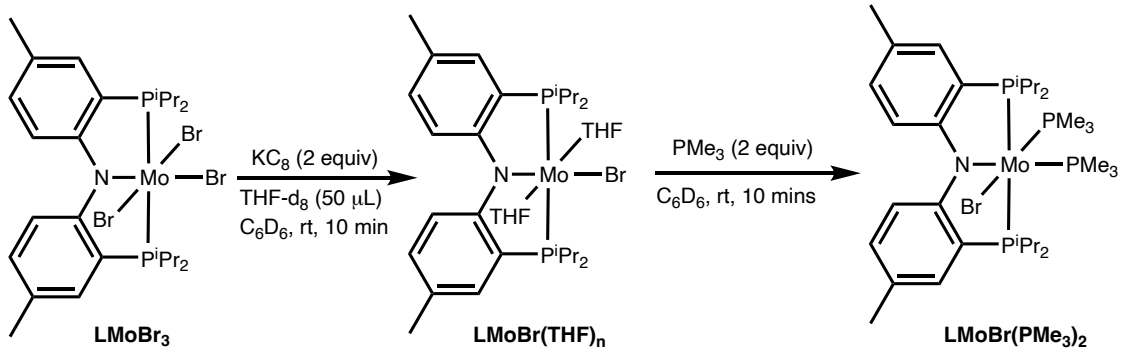

LMoBr$_3$ **LMoBr(THF)$_n$** **LMoBr(PMe$_3$)$_2$**

To a J. Young NMR tube, **LMoBr$_3$** (7.6 mg, 0.010 mmol, 1.0 equiv) was weighed and dissolved in 0.5 mL of C_6D_6. To this solution 50 μL of THF-d_8 and then KC_8 (2.7 mg, 0.020 mmol K, 2.0 equiv) were added and the mixture was shaken. When the color changed to dark purple the ^{1}H NMR spectrum was recorded and formation of **LMoBr(THF)$_n$** was confirmed. To this solution PMe_3 (2.0 μL, 0.020 mmol, 2 equiv) was added and the color immediately changed to violet. Only NMR signals attributed to paramagnetic species were observed.

^{1}H NMR: (C_6D_6, 500 MHz): (all paramagnetic chemical shifts): δ 74.9, 50.2, 24.9, 15.3, 12.1, 9.4, -6.8, -7.5, -14.7, -33.4.

The magnetic susceptibility was determined by the Evans method to be 2.9 μ_B.

S2.3.2 Reduction of $LMoBr_3$ in other coordinating solvents

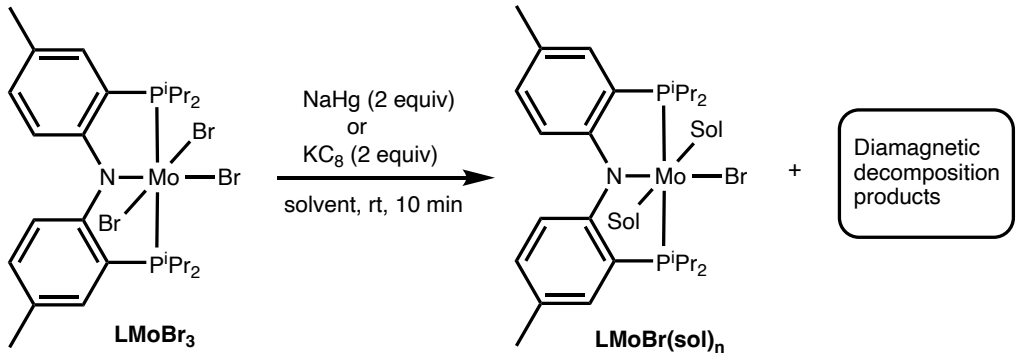

CD_3CN: To a J. Young NMR tube, **$LMoBr_3$** (7.6 mg, 0.010 mmol, 1.0 equiv) was weighed and dissolved in 0.5 mL of CD_3CN. To this solution either KC_8 (2.7 mg, 0.020 mmol K, 2.0 equiv) or 0.5 w/w% sodium amalgam (Na/Hg) (92.0 mg, 0.020 mmol Na, 2.0 equiv) was added and the mixture was shaken vigorously. The color changed to a green-brown and ^1H NMR and $^{31}P\{^1H\}$ NMR spectra were recorded. Several resonances indicative of paramagnetic species were observed in the ^1H NMR spectrum, along with peaks indicative of several diamagnetic products observed in the ^1H and $^{31}P\{^1H\}$ NMR spectra. DFT studies indicate that the ground state of **$LMoBr(CH_3CN)_2$** is a triplet; this may explain the paramagnetic signals in the ^1H NMR spectrum. However, formation of **1** was never observed in the presence of CD_3CN.

^1H NMR: (CD_3CN, 500 MHz): (all paramagnetic chemical shifts): δ 71.9, 63.7, 58.2, 54.8, 32.2, 25.6, 23.5, 11.5, -15.8.

Diethyl ether/Dioxane: When the same reaction was performed in diethyl ether and dioxane, the color changed to a red-purple solution. The solvent was then evaporated, and the ^1H NMR spectrum in either C_6D_6 or THF-d_8 reveals formation of Mo-oxo as the major decomposition product (see S2.3.3)

S2.3.3 Reduction of $LMoBr_3$ in non-coordinating solvent (not rigorously dry)

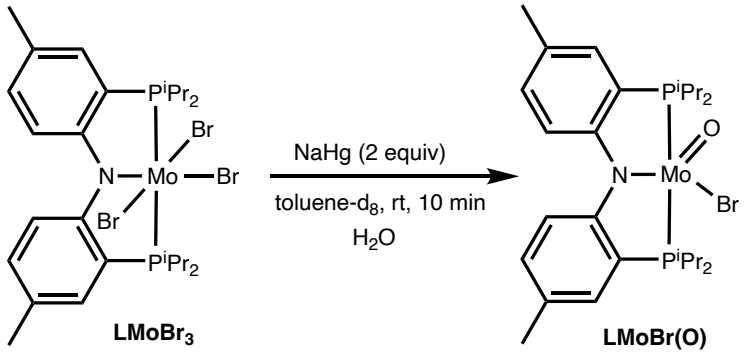

To a J. Young NMR tube, **$LMoBr_3$** (7.6 mg, 0.010 mmol, 1.0 equiv) was weighed and dissolved in 0.5 mL of toluene-d_8 (1 mL ampules, bought from CIL, contains H_2O). To this solution 0.5 w/w% sodium amalgam (Na/Hg) (92.0 mg, 0.020 mmol Na, 2.0 equiv) was added and the mixture was shaken vigorously. The solution color changed to brown and the ^{1}H NMR and $^{31}P\{^1H\}$ NMR spectra were recorded. The formation of complex **1** was not observed. Two broad peaks at 68.9 and 54.1 ppm appeared in the $^{31}P\{^1H\}$ NMR spectrum. Cooling this sample to -45 °C revealed an AB pattern with peaks at 68.4 and 54.5 ppm and with J = 100 Hz (See Figure S18). A crystal of **LMoBr(O)** was obtained via slow diffusion of diethyl ether or pentane to a saturated toluene solution under argon atmosphere (S3.3; Figure S3)

On multiple occasions we have obtained the same crystal structure with the same NMR spectrum. Numerous attempts to crystalize **$LMoBr(THF)_n$** or **$LMoBr(sol)_n$** afforded **LMoBr(O)** crystals. When the same reaction was performed in the presence of NaI, crystals were formed and crystallographically characterized as **LMoI(O)** (S3.4; Figure S4).

^{1}H NMR: (Toluene-d_8, 500 MHz): δ 6.94 (d, J = 7.4 Hz, 3H), 6.74 (d, J = 8.4 Hz, 3H), 2.86 – 2.59 (m, 2H), 2.14 (s, 6H), 1.83 – 1.60 (m, 2H), 1.36 (dd, J = 16.5, 6.8 Hz, 6H), 1.13 – 1.05 (m, 12H), 1.00 (dd, J = 15.9, 6.5 Hz, 6H).

$^{31}P\{^1H\}$ NMR: (Toluene-d_8, 202 MHz): (at 25 °C) δ 68.8 (br, s), 54.2 (br, s).

(at -45 °C) δ 68.4 (d, J = 100.6 Hz), 54.4 (d, J = 100.1 Hz).

III. Crystallographic data

S3.1 Crystallographic data for **1**

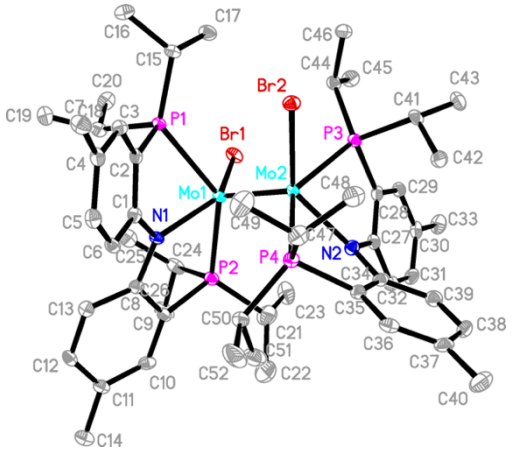

Figure S1. ORTEP representation (50% probability ellipsoids) of the structure of **1** determined by X-ray diffraction; hydrogen atoms were omitted for clarity.

Table S1. Crystal data and structure refinement for SM_122_twin4_P-1.

Identification code	SM_122_twin4_P-1	
Empirical formula	C52 H80 Br2 Mo2 N2 P4	
Formula weight	1208.76	
Temperature	120(2) K	
Wavelength	0.71073 Å	
Crystal system	Triclinic	
Space group	P-1	
Unit cell dimensions	a = 11.3371(8) Å	α= 80.153(2)°.
	b = 12.9335(10) Å	β= 73.6830(10)°.
	c = 20.1041(15) Å	γ = 69.5740(10)°.
Volume	2642.5(3) Å^3	
Z	2	
Density (calculated)	1.519 Mg/m^3	
Absorption coefficient	2.144 mm^{-1}	
F(000)	1240	
Crystal size	0.200 x 0.200 x 0.100 mm^3	
Theta range for data collection	1.686 to 25.917°.	
Index ranges	-13<=h<=13, -15<=k<=15, 0<=l<=24	
Reflections collected	16605	
Independent reflections	10064 [R(int) = 0.0305]	
Completeness to theta = 25.242°	99.8 %	
Absorption correction	Semi-empirical from equivalents	
Max. and min. transmission	0.7452 and 0.3184	
Refinement method	Full-matrix least-squares on F^2	
Data / restraints / parameters	10064 / 0 / 579	
Goodness-of-fit on F^2	1.005	
Final R indices [I>2sigma(I)]	R1 = 0.0357, wR2 = 0.0830	
R indices (all data)	R1 = 0.0469, wR2 = 0.0863	
Extinction coefficient	n/a	
Largest diff. peak and hole	1.137 and -0.987 e.Å^{-3}	

S3.2 Crystallographic data for **LMoI(CO)$_2$**

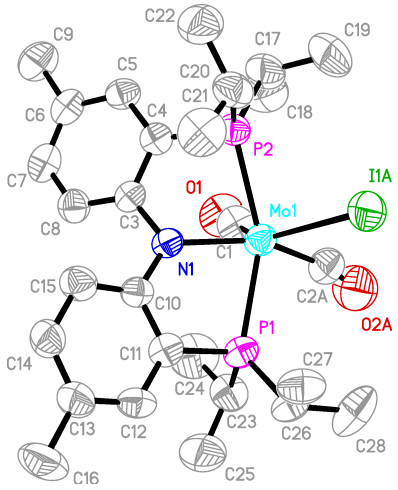

Figure S2. ORTEP representation (50% probability ellipsoids) of the structure of **LMoI(CO)$_2$** determined by X-ray diffraction; hydrogen atoms were omitted for clarity.

Table S2. Crystal data and structure refinement for sm_120_B.

Identification code	sm_120_B	
Empirical formula	C28 H40 I Mo N O2 P2	
Formula weight	707.39	
Temperature	120(2) K	
Wavelength	0.71073 Å	
Crystal system	Orthorhombic	
Space group	$Pca2_1$	
Unit cell dimensions	a = 17.857(7) Å	α= 90°.
	b = 10.099(4) Å	β= 90°.
	c = 17.473(5) Å	γ = 90°.
Volume	3151(2) Å^3	
Z	4	
Density (calculated)	1.491 Mg/m^3	
Absorption coefficient	1.521 mm^{-1}	
F(000)	1424	
Crystal size	0.150 x 0.100 x 0.070 mm^3	
Theta range for data collection	2.016 to 25.679°.	
Index ranges	-16<=h<=21, -12<=k<=12, -18<=l<=21	
Reflections collected	24381	
Independent reflections	5466 [R(int) = 0.0832]	
Completeness to theta = 25.242°	99.5 %	
Absorption correction	None	
Refinement method	Full-matrix least-squares on F^2	
Data / restraints / parameters	5466 / 583 / 345	
Goodness-of-fit on F^2	1.112	
Final R indices [I>2sigma(I)]	R1 = 0.0932, wR2 = 0.2157	
R indices (all data)	R1 = 0.1301, wR2 = 0.2372	
Absolute structure parameter	0.03(4)	
Extinction coefficient	n/a	
Largest diff. peak and hole	2.241 and -0.941 e.Å^{-3}	

S3.3 Crystallographic data for **LMoBr(O)**

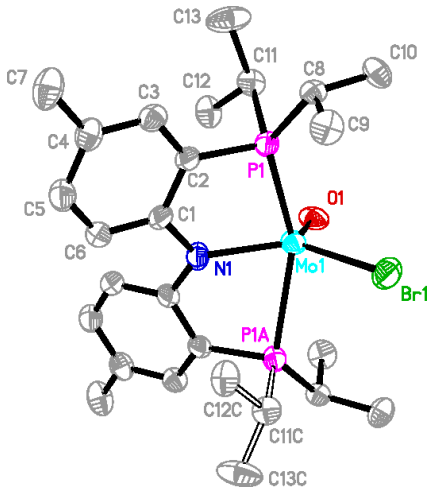

Figure S3. ORTEP representation (50% probability ellipsoids) of the structure of **LMoBr(O)** determined by X-ray diffraction; hydrogen atoms were omitted for clarity.

Table S3. Crystal data and structure refinement for SM-882a_faces.

Identification code	SM-882	
Empirical formula	C26 H40 Br Mo N O P2	
Formula weight	620.38	
Temperature	120(2) K	
Wavelength	1.54184 Å	
Crystal system	Monoclinic	
Space group	P2/n	
Unit cell dimensions	a = 11.4244(3) Å	α= 90°.
	b = 9.5870(3) Å	β= 97.018(2)°.
	c = 12.5215(3) Å	γ = 90°.
Volume	1361.15(6) Å^3	
Z	2	
Density (calculated)	1.514 Mg/m^3	
Absorption coefficient	6.906 mm^{-1}	
F(000)	636	
Crystal size	0.242 x 0.137 x 0.021 mm^3	
Theta range for data collection	4.612 to 70.074°.	
Index ranges	-13<=h<=13, -11<=k<=11, -15<=l<=11	
Reflections collected	12854	
Independent reflections	2580 [R(int) = 0.0413]	
Completeness to theta = 67.684°	99.8 %	
Absorption correction	Gaussian	
Max. and min. transmission	1.000 and 0.503	
Refinement method	Full-matrix least-squares on F^2	
Data / restraints / parameters	2580 / 350 / 175	
Goodness-of-fit on F^2	1.050	
Final R indices [I>2sigma(I)]	R1 = 0.0512, wR2 = 0.1475	
R indices (all data)	R1 = 0.0540, wR2 = 0.1497	
Extinction coefficient	n/a	
Largest diff. peak and hole	0.816 and -0.650 e.Å^{-3}	

S3.4 Crystallographic data for **LMoI(O)**

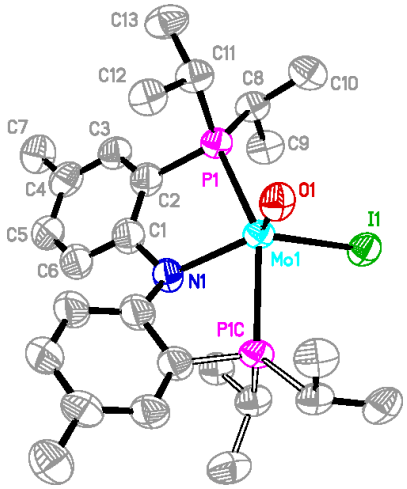

Figure S4. ORTEP representation (50% probability ellipsoids) of the structure of **LMoI(O)** determined by X-ray diffraction; hydrogen atoms were omitted for clarity.

Table S4. Crystal data and structure refinement for SM-358-red_twin1_2_b.

Identification code	SM-358	
Empirical formula	C26 H40 I Mo N O P2	
Formula weight	667.37	
Temperature	100(2) K	
Wavelength	1.54184 Å	
Crystal system	Monoclinic	
Space group	P2/n	
Unit cell dimensions	a = 11.4773(5) Å	α= 90°.
	b = 9.9829(5) Å	β= 97.277(4)°.
	c = 12.2032(5) Å	γ = 90°.
Volume	1386.94(11) $Å^3$	
Z	2	
Density (calculated)	1.598 Mg/m^3	
Absorption coefficient	13.829 mm^{-1}	
F(000)	672	
Crystal size	0.160 x 0.070 x 0.060 mm^3	
Theta range for data collection	4.429 to 68.248°.	
Index ranges	-10<=h<=13, -12<=k<=10, -14<=l<=14	
Reflections collected	12835	
Independent reflections	2523 [R(int) = 0.0914]	
Completeness to theta = 67.684°	99.4 %	
Absorption correction	Sphere	
Max. and min. transmission	0.48980 and 0.43777	
Refinement method	Full-matrix least-squares on F^2	
Data / restraints / parameters	2523 / 382 / 193	
Goodness-of-fit on F^2	1.189	
Final R indices [I>2sigma(I)]	R1 = 0.0740, wR2 = 0.2009	
R indices (all data)	R1 = 0.0773, wR2 = 0.2029	
Extinction coefficient	n/a	
Largest diff. peak and hole	1.157 and -0.742 $e.Å^{-3}$	

IV. NMR spectra

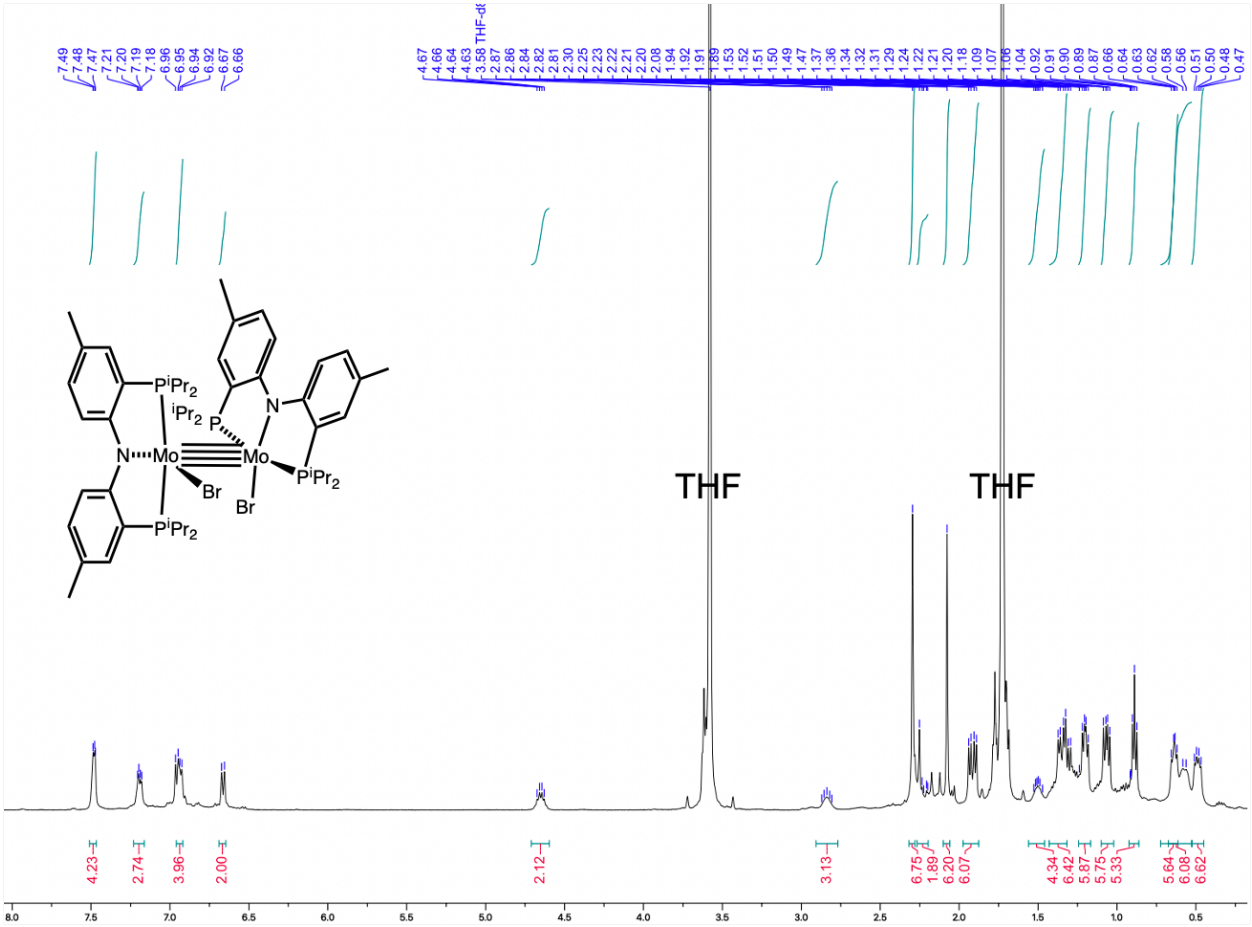

Figure S5. ^{1}H NMR spectrum of **1**

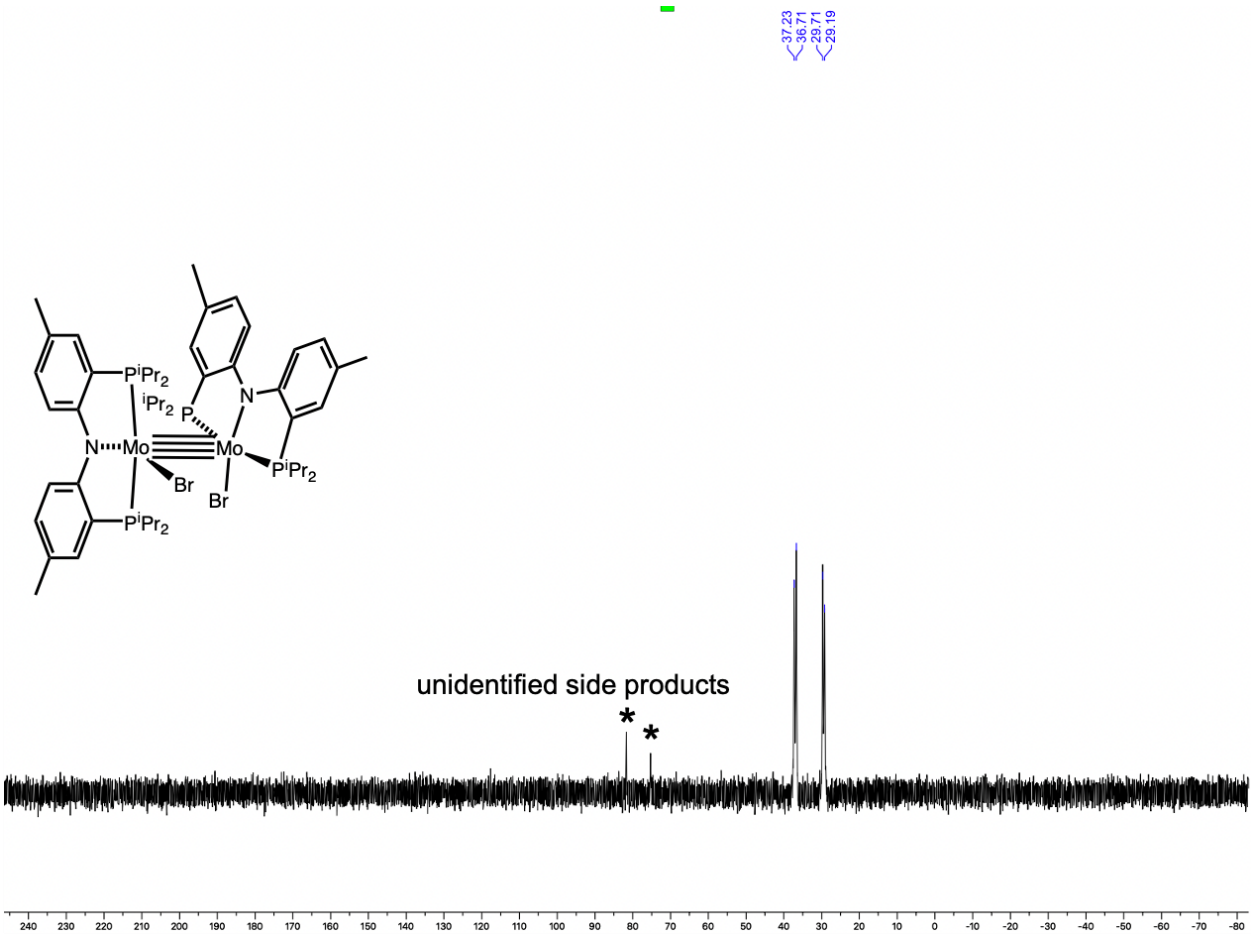

Figure S6. $^{31}P\{^{1}H\}$ NMR spectrum of **1**

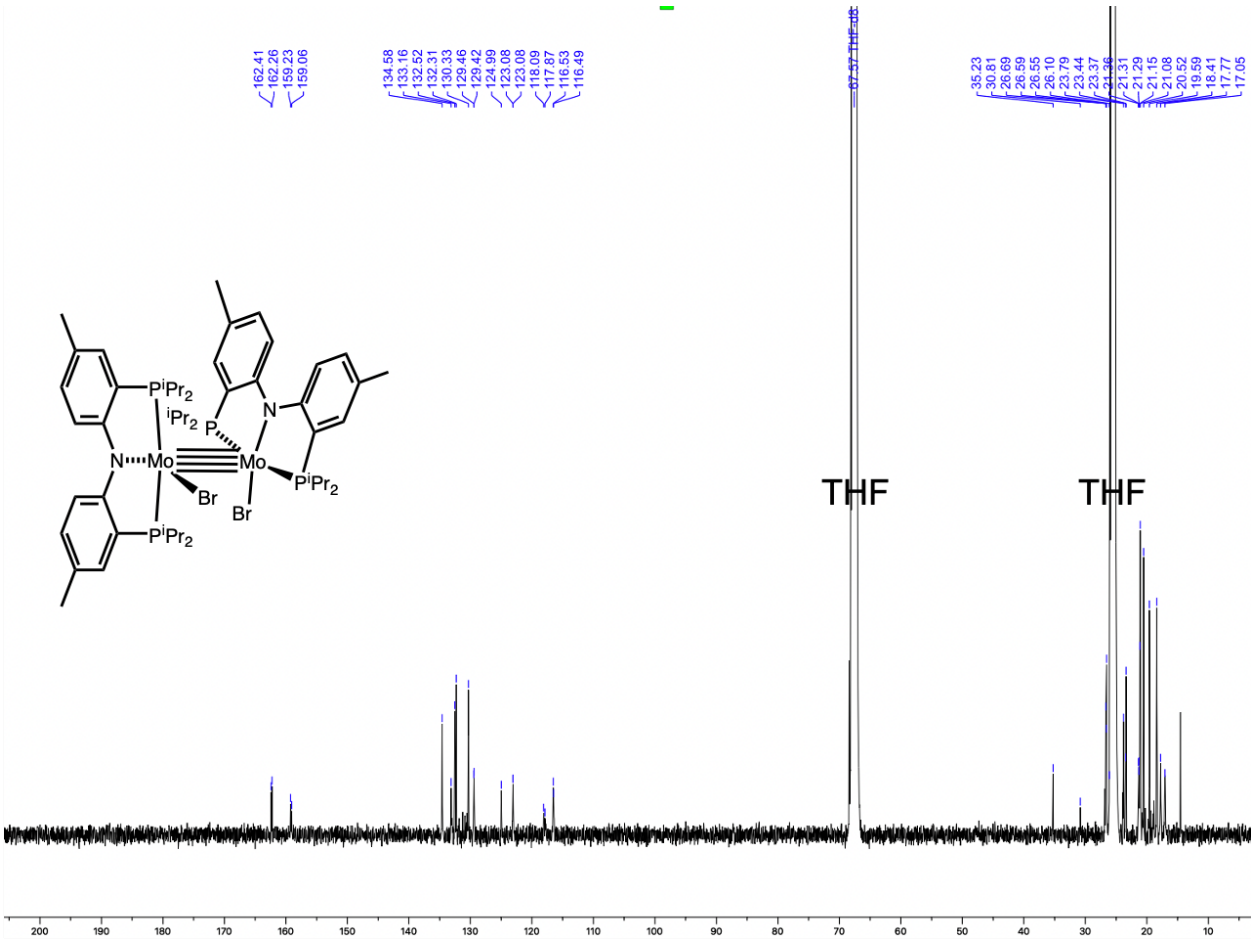

Figure S7. $^{13}C\{^{1}H\}$ NMR spectrum of **1**

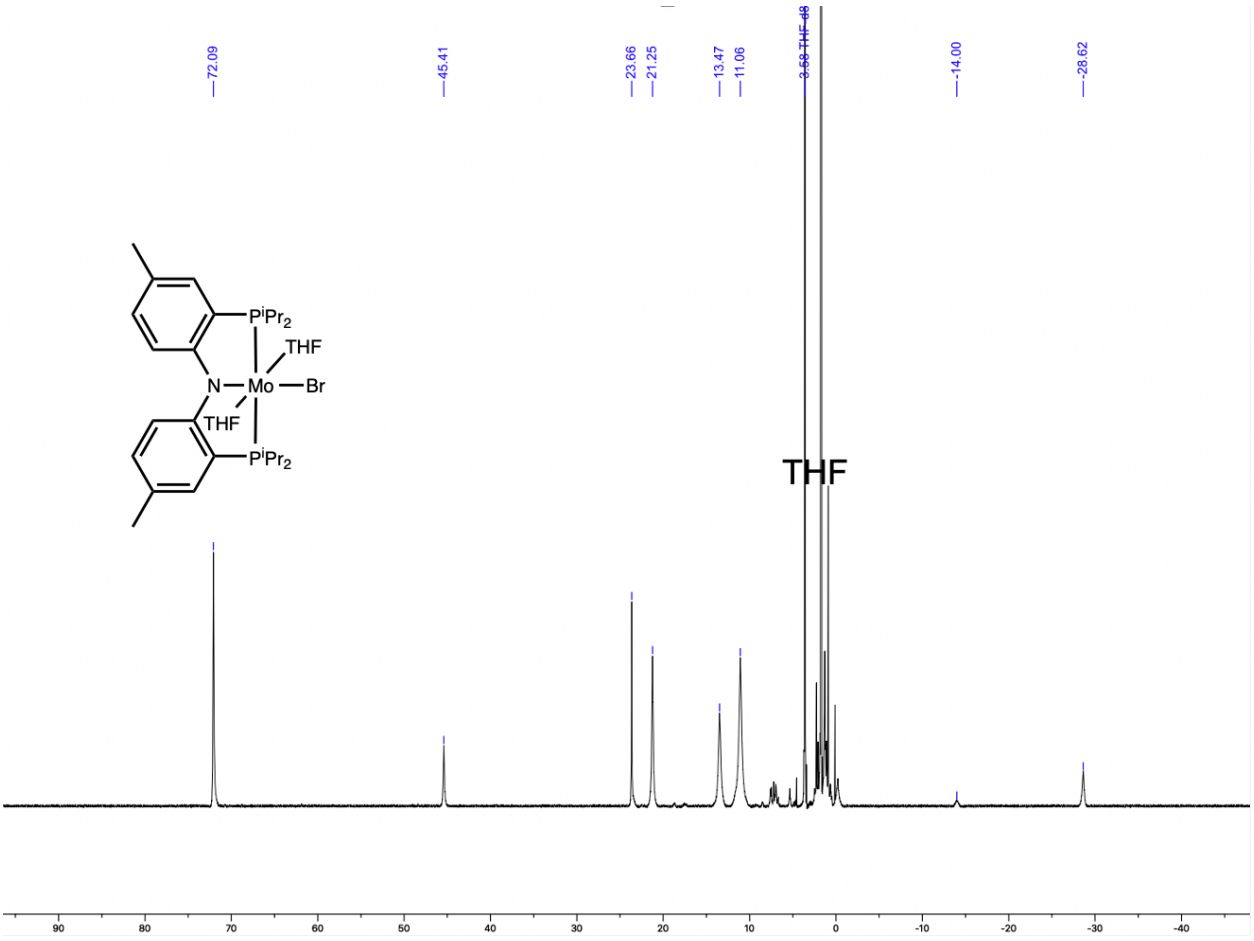

Figure S8. ^{1}H NMR spectrum of **LMoBr(THF)$_n$** (paramagnetic resonances)

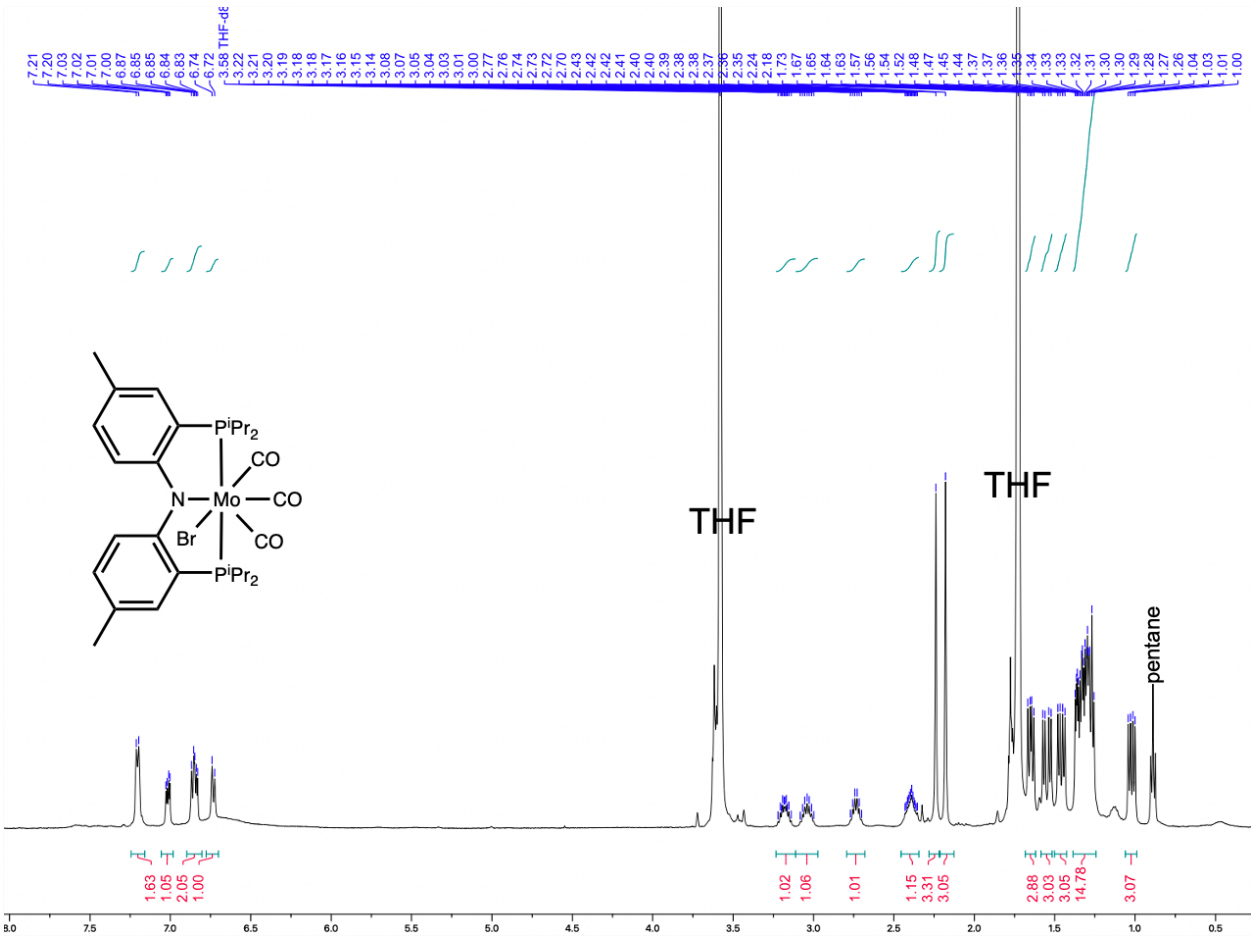

Figure S9. ^{1}H NMR spectrum of **LMoBr(CO)$_3$**

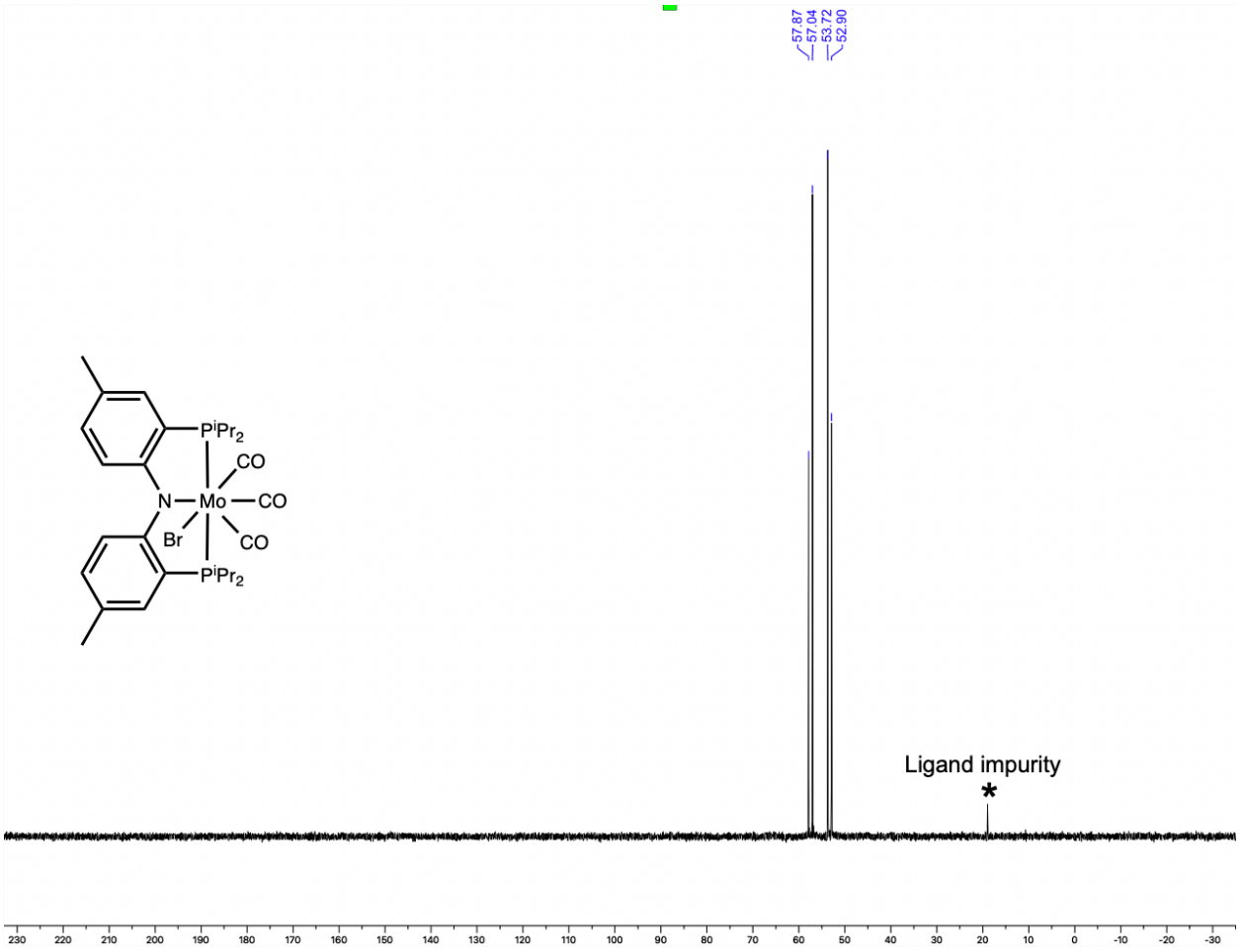

Figure S10. $^{31}P\{^{1}H\}$ NMR spectrum of **LMoBr(CO)$_3$** (with ligand impurities)

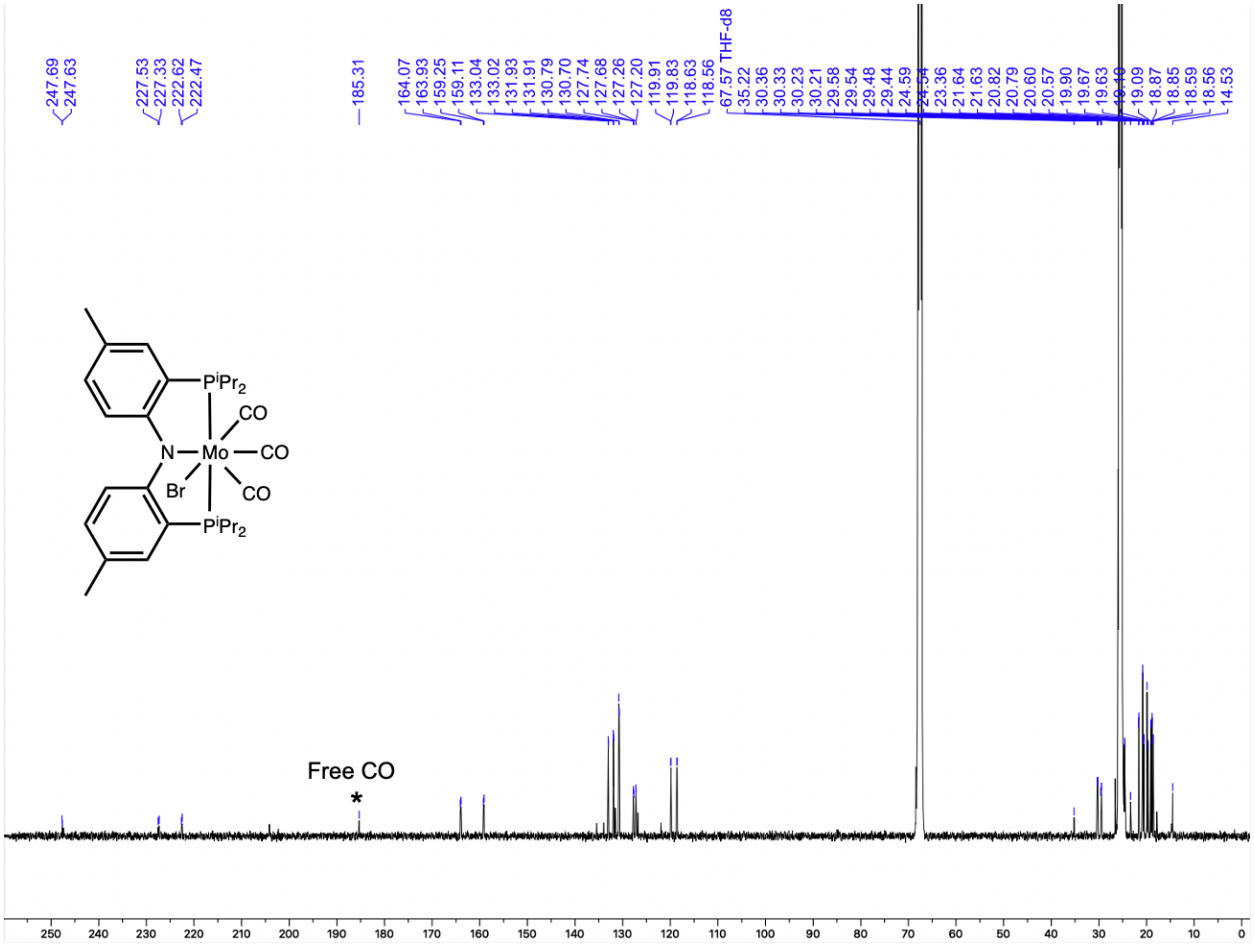

Figure S11. $^{13}C\{^{1}H\}$ NMR spectrum of **LMoBr(CO)$_3$**

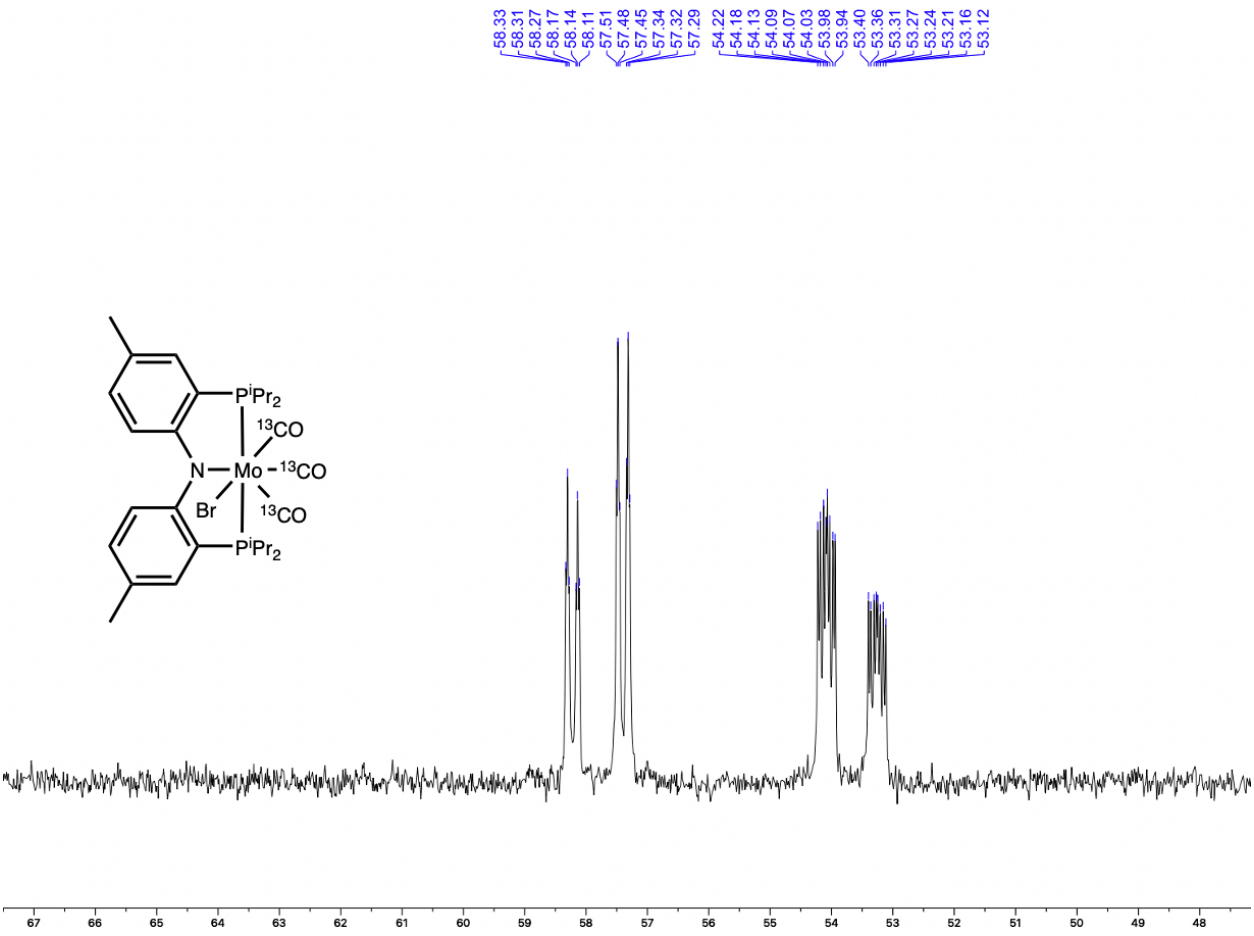

Figure S12. $^{31}P\{^{1}H\}$ NMR spectrum of **LMoBr(^{13}CO)$_3$**

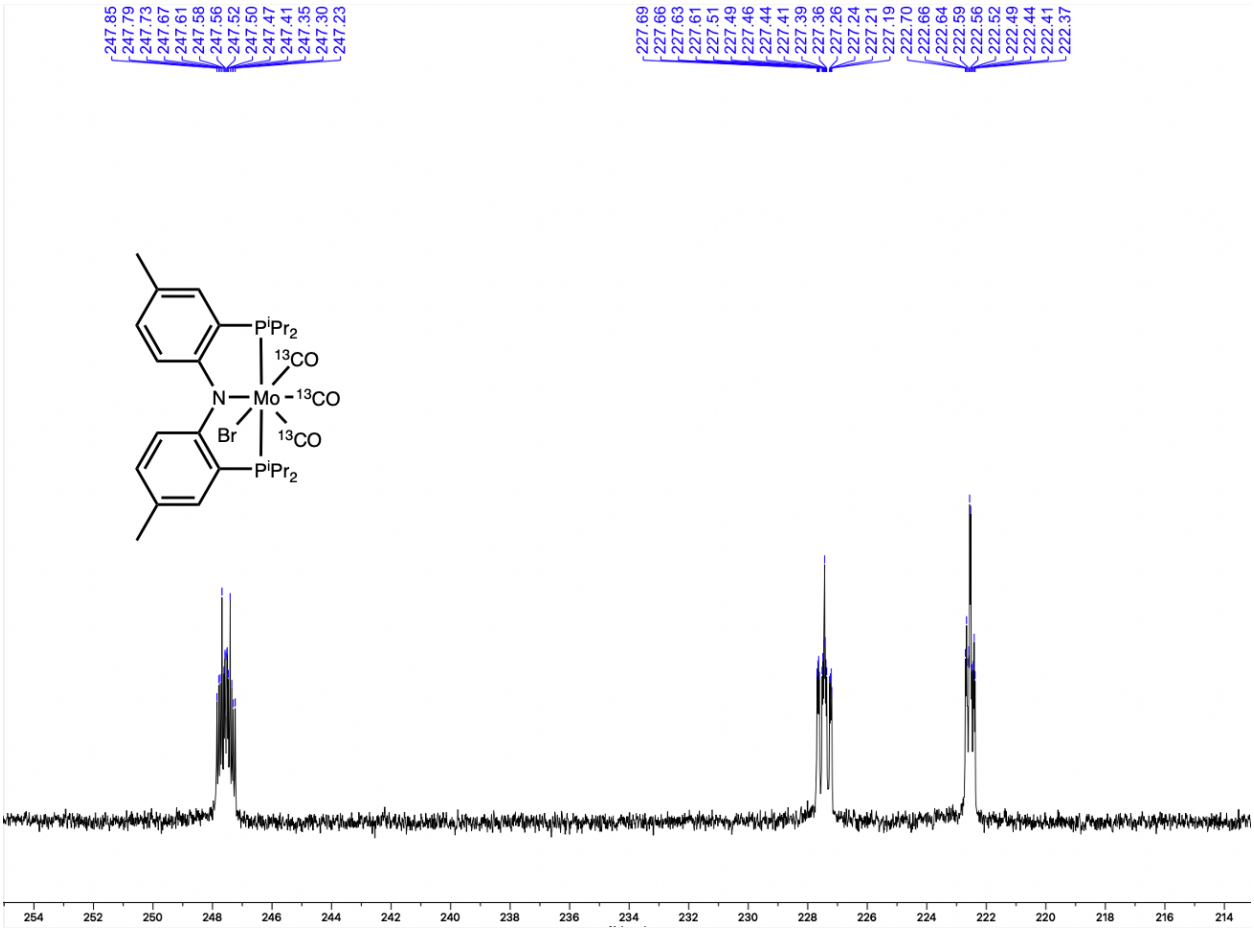

Figure S13. $^{13}C\{^{1}H\}$ NMR spectrum of **LMoBr(^{13}CO)$_3$** (carbonyl region only)

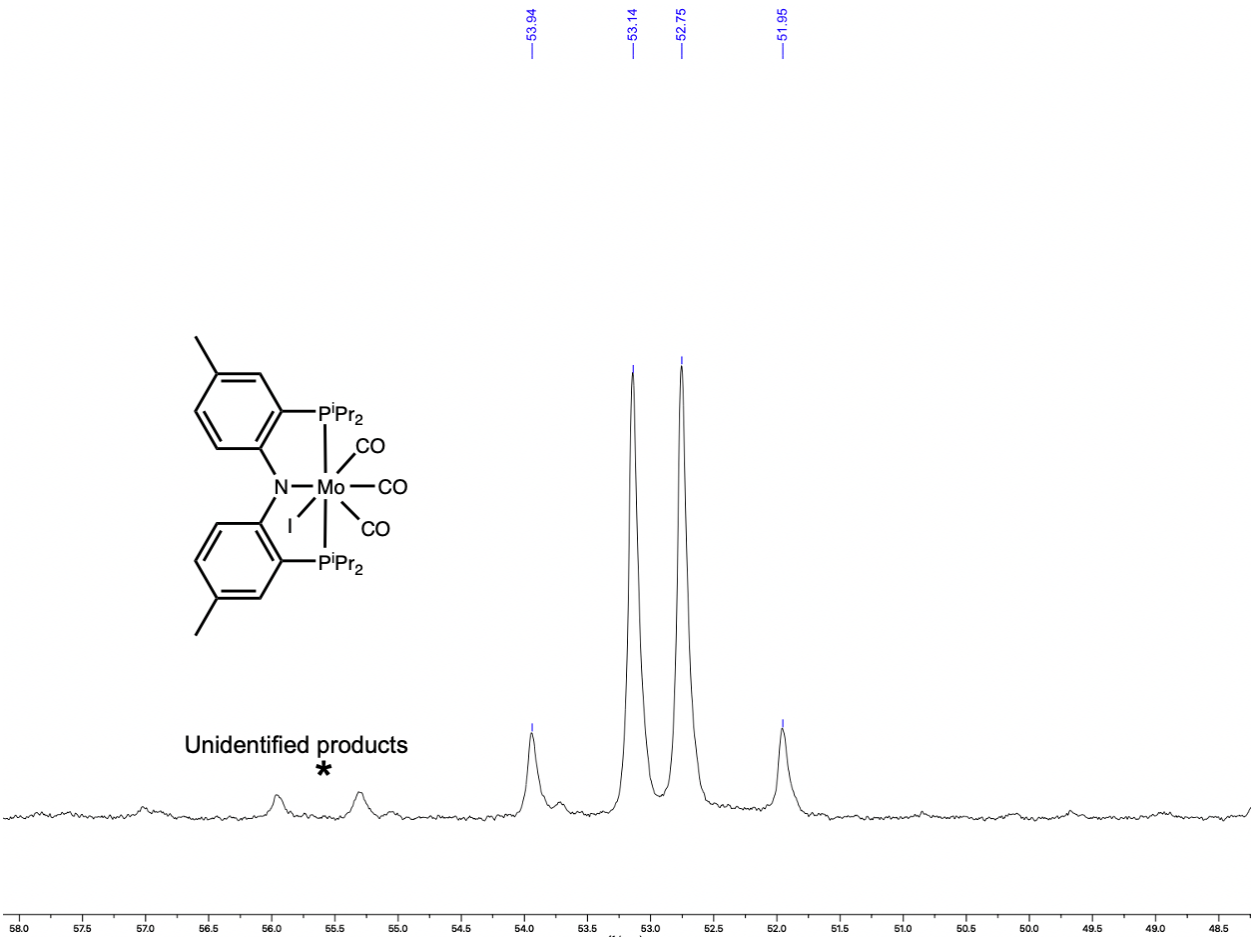

Figure S14. $^{31}P\{^{1}H\}$ NMR spectrum of **LMoI(CO)$_3$** (with an unidentified minor product)

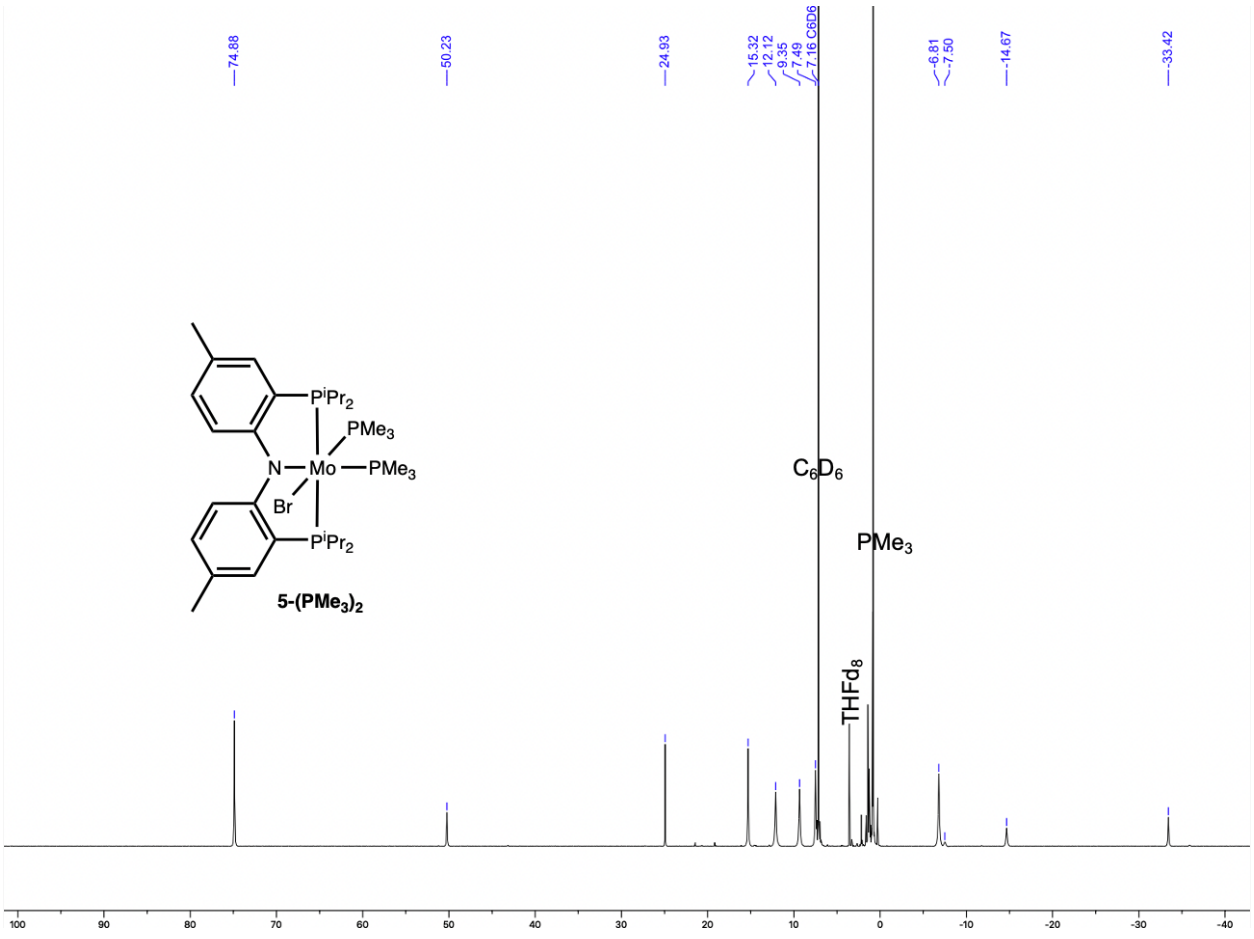

Figure S15. ^{1}H NMR spectrum of **LMoBr(PMe$_3$)$_2$**

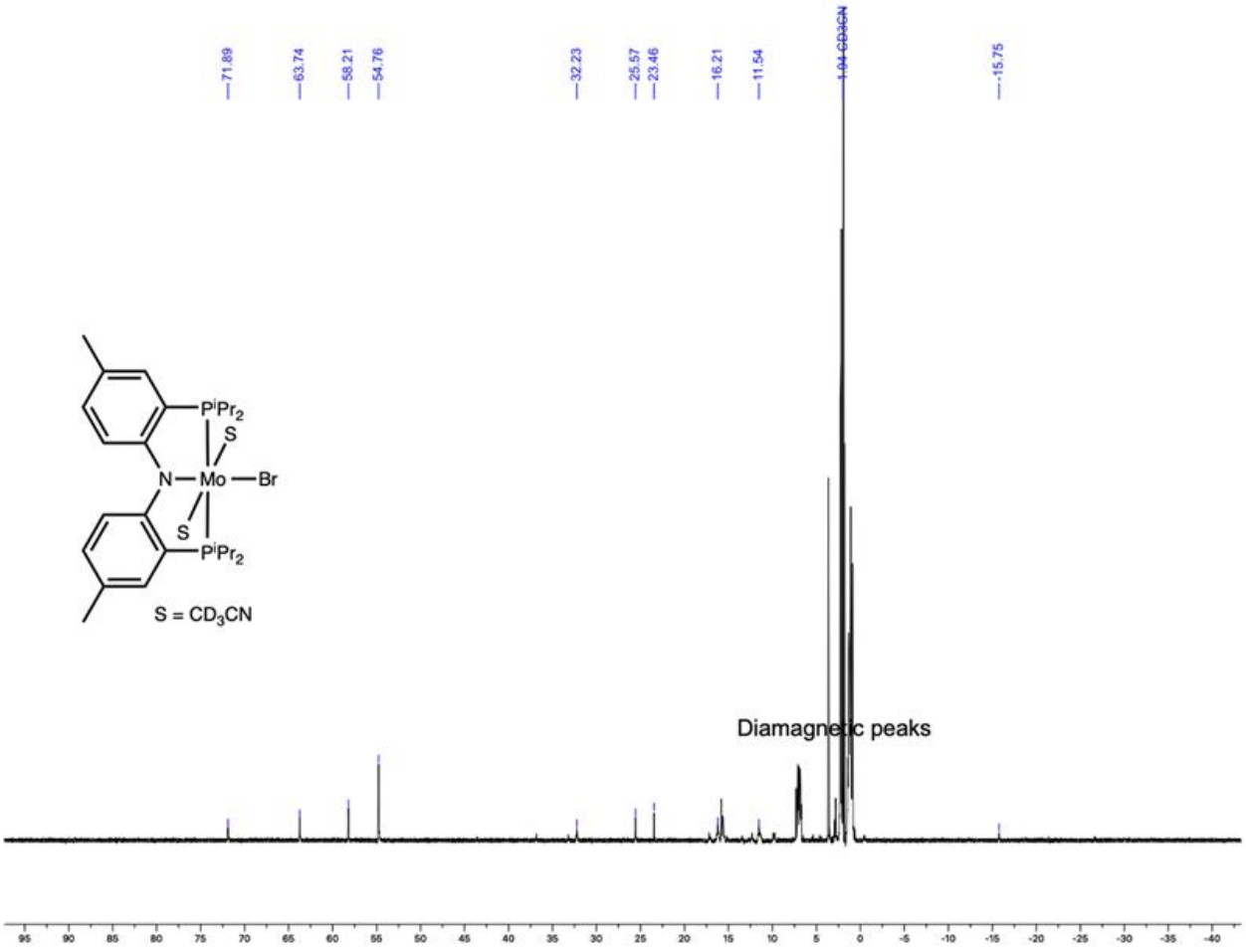

Figure S16. ^{1}H NMR spectrum of **LMoBr(CD$_3$CN)$_n$**

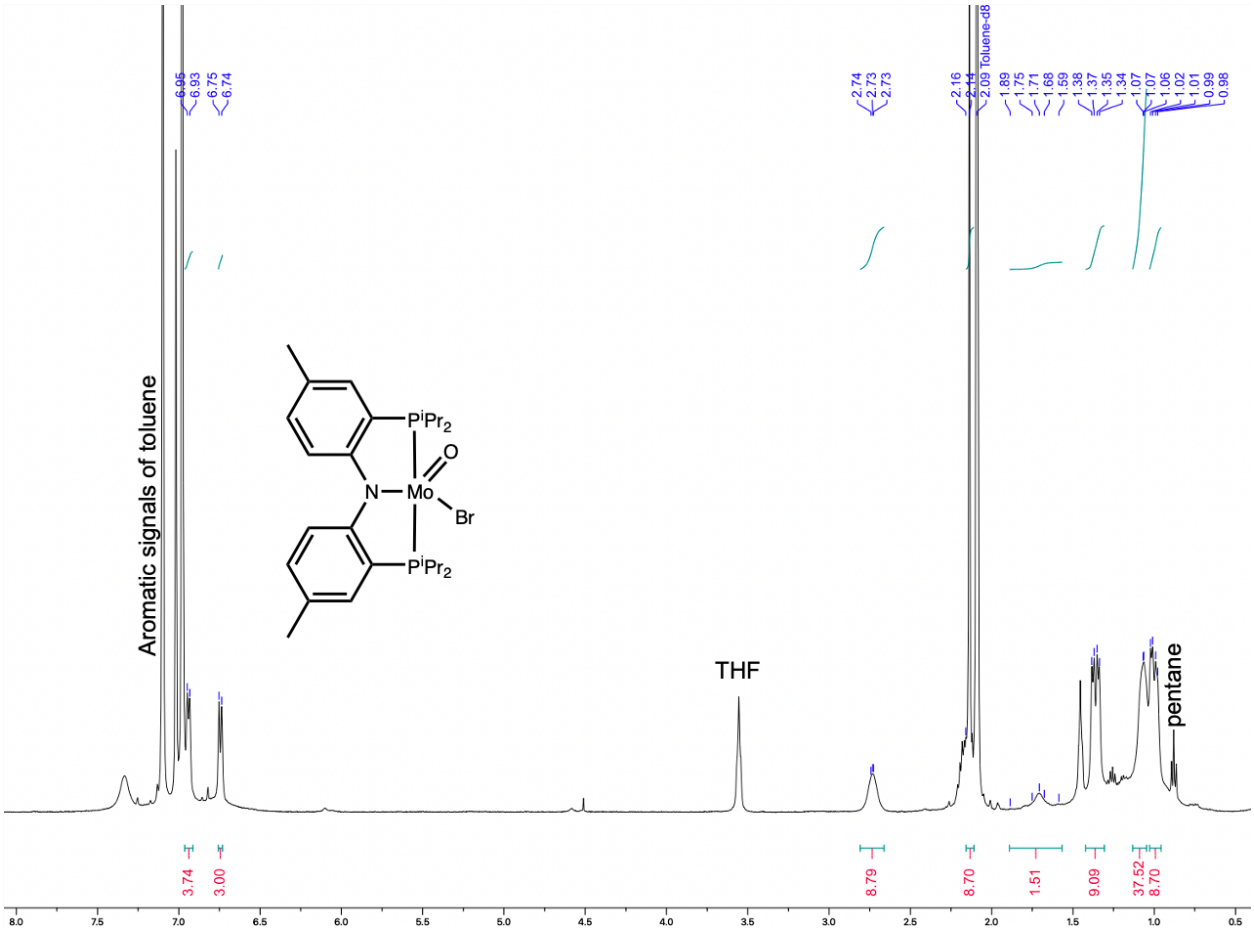

Figure S17. ^{1}H NMR spectrum of **LMoBr(O)**

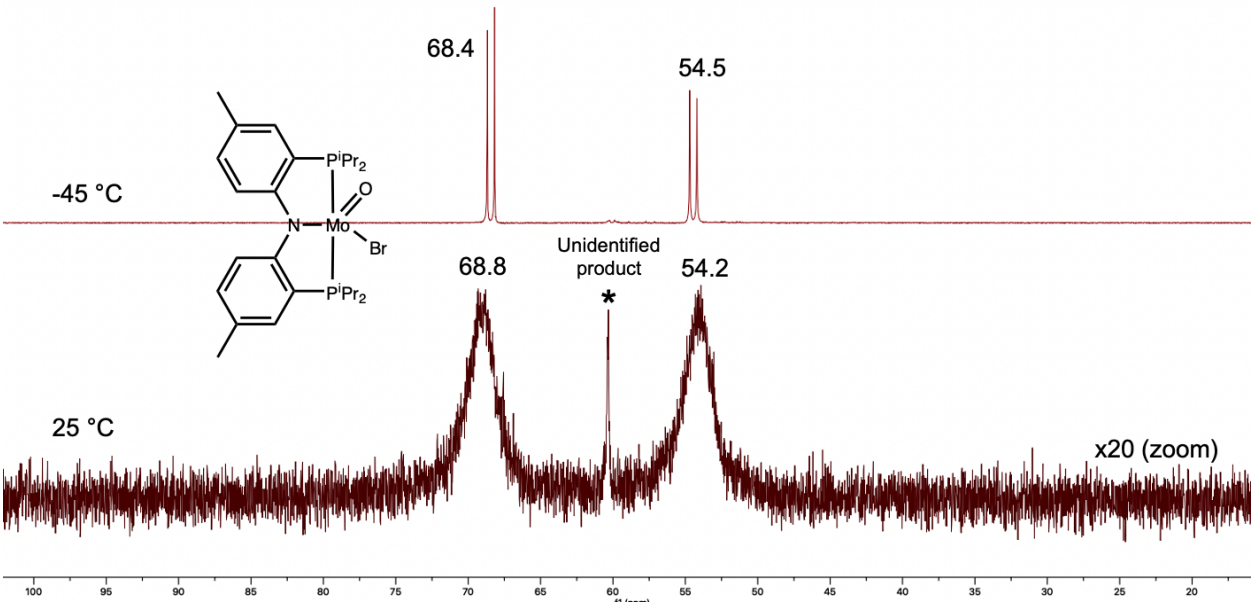

Figure S18. Stacked ^{31}P{^{1}H} NMR spectra of **LMoBr(O)** at 25 °C (below) and -45 °C (above)

V. Computational methods and results

Electronic structure calculations based on Density Functional Theory (DFT) were done using Gaussian 16 (rev A03)[S12]. The graphical interface GaussView 6.0 was used to prepare initial input structures and analyze the output files. Geometry optimization and vibrational analysis were done in the gas phase using the M06 global hybrid exchange-correlation functional[S13,S14] with the Pople-type split valence plus polarization basis set[S15-S18] 6-311g** on light atoms and Stuttgart-Dresden (SDD)[S19] effective core potentials and basis set on Mo and Br. Final electronic and solvation energies were obtained by single point calculations in the SMD continuum solvation model on the gas-phase geometries using both the M06-D3[S14,S20] and the B3LYP-D3BJ[S21,S22] density functional, with added Grimme's dispersion correction terms.[S23] These calculations used the Ahlrichs def2-tzvp basis set[S24,S25] on the main group atoms and the def2-qzvp basis set with associated ECP[S26] on Mo and Br. The final electronic energy for free CO did not include SMD continuum solvation effects. Correction terms to the enthalpy and Gibbs free energy were determined at 1.0 atm and 298 K using unscaled gas phase vibrational frequencies, while scaling the gas phase translational and rotational entropies by 0.6.[S27] All computations on non-singlet spin states employed the "guess=mix" keyword

S5.1 Thermodynamics of formation of 1 from (P^{Ar}NP)MoBr (LMoBr)

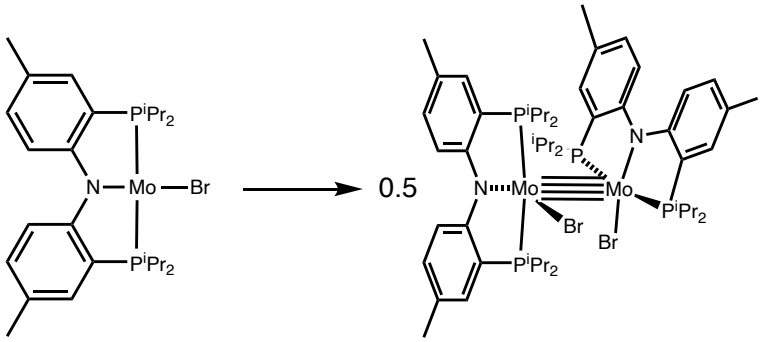

M06D3			B3LYP-D3BJ		
ΔE	ΔH	ΔG[a]	ΔE	ΔH	ΔG[a]
-27.7	-25.8	-16.7	-28.9	-27.0	-17.9

[a] Values after scaling translational and rotational entropies.

S5.2 Thermodynamics of formation of pincer-ligated quadruply-bonded Mo–Mo dimers from monomeric units

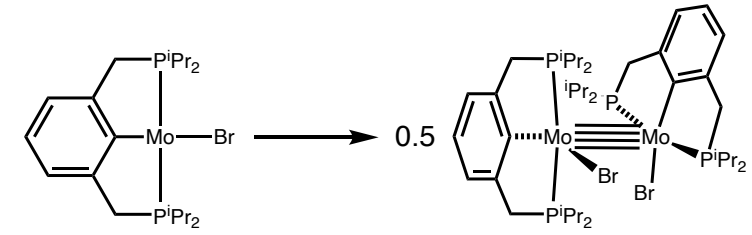

[(^{iPr}PCP)MoBr]$_2$

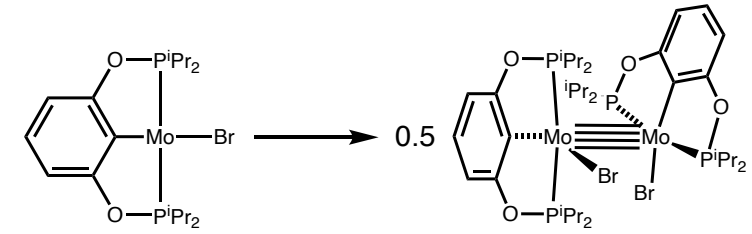

[(^{iPr}POCOP)MoBr]$_2$

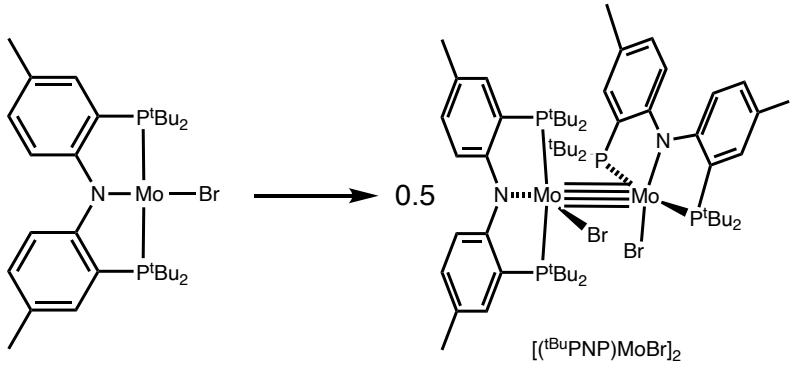

[(^{tBu}PNP)MoBr]$_2$

All values in kcal/mol		M06D3			B3LYP-D3BJ		
Species	**Spin state**	ΔE	ΔH	ΔG[a]	ΔE	ΔH	ΔG[a]
[(^{iPr}PCP)MoBr]$_2$	Singlet	-37.4	-35.5	-27.0	-39.5	-37.5	-29.0
[(^{iPr}POCOP)MoBr]$_2$	Singlet	-33.7	-31.9	-23.4	-36.1	-34.3	-25.8
[(^{tBu}PNP)MoBr]$_2$	Singlet	3.4	6.3	14.3	4.3	7.2	15.2

[a] Values after scaling translational and rotational entropies.

S5.3 Thermodynamics of addition of one or two L ligands to ($P^{Ar}NP$)MoBr

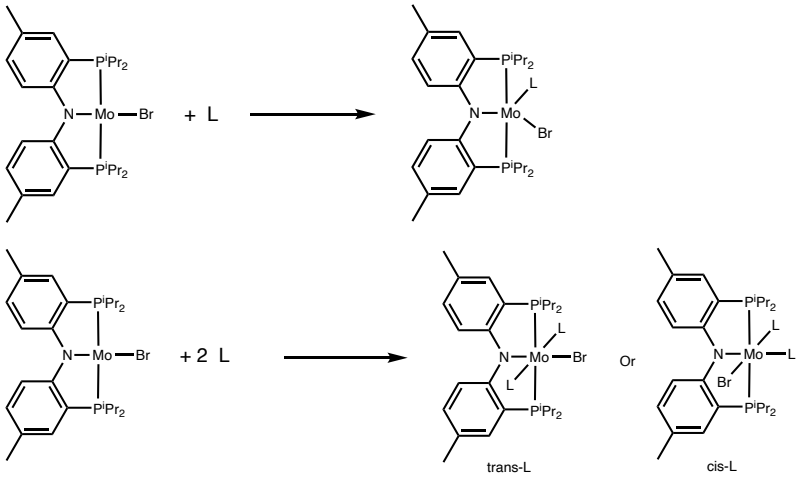

All values in kcal/mol		M06D3			B3LYP-D3BJ		
Species	**Spin state**	ΔE	ΔH	ΔG[a]	ΔE	ΔH	ΔG[a]
***cis*-LMoBr(CO)$_2$**	Quintet	1.9	2.8	26.6	-2.7	-1.8	22.0
	Triplet	-59.8	-57.2	-31.4	-66.1	-63.4	-37.6
	Singlet	-70.0	-66.4	-40.5	-75.8	-72.3	-46.4
***trans*-LMoBr(CO)$_2$**	Quintet	-13.6	-11.8	11.4	-13.8	-12.0	11.2
	Triplet	-62.9	-59.8	-36.1	-69.2	-66.1	-42.4
	Singlet	-63.5	-60.3	-35.8	-69.7	-66.5	-42.0
***cis*-LMoBr(PMe$_3$)$_2$**	Quintet	-22.4	-19.4	-6.7	-14.7	-11.7	1.1
	Triplet	-43.1	-38.0	-21.3	-45.1	-40.1	-23.4
	Singlet	-37.2	-32.6	-14.4	-38.9	-34.3	-16.1
***trans*-LMoBr(PMe$_3$)$_2$**	Quintet	-28.1	-25.1	-12.9	-19.4	-16.4	-4.2
	Triplet	-43.6	-39.2	-22.5	-45.2	-40.8	-24.1
	Singlet	-32.3	-27.2	-8.8	-33.2	-28.1	-9.7
LMoBr(THF)	Quintet	-2.9	-1.0	0.2[b]	2.5	4.4	5.6[b]
	Triplet	8.2	10.3	12.4[b]	12.4	14.5	16.5[b]
	Singlet	12.5	14.3	18.4[b]	11.6	13.5	17.6[b]
LMoBr(THF)•THF[c]	Quintet	-23.3	-19.0	-16.2[b]	-12.7	-8.3	-5.6[b]
***cis*-LMoBr(THF)$_2$**	Triplet	-17.8	-13.3	-8.3[b]	-15.9	-11.5	-6.4[b]
	Singlet	-13.9	-10.0	-1.8[b]	-11.7	-7.8	0.4[b]
***trans*-LMoBr(THF)$_2$**	Quintet	-20.7	-17.8	-12.6[b]	-9.1	-6.3	-1.1[b]

	Triplet	-21.5	-16.8	-10.7[b]	-19.6	-14.9	-8.8[b]
	Singlet	-10.7	-6.5	2.6[b]	-8.9	-4.8	4.4[b]

[a]Values after scaling translational and rotational entropies.

[b]Values including statistical correction for concentration of THF solvent.

[c]Repeated attempts to optimize a quintet state of *cis*-**LMo**Br(THF)$_2$ led to the decoordination of one THF ligand and to a complex **LMo**Br(THF)•THF in which the O atom of the non-coordinated THF molecule is H-bonded to an α-C–H bond of the coordinated molecule of THF.

S5.4 Thermodynamics of $[LMoBr_2]_2$ formation

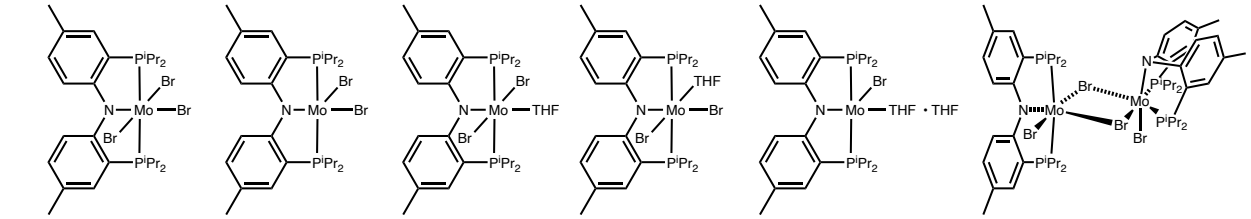

All values in kcal/mol	M06D3			B3LYP-D3BJ		
Reaction	ΔE	ΔH	ΔG[a]	ΔE	ΔH	ΔG[a]
LMoBr$_2$ + THF → **trans-LMoBr$_2$(THF)**	-31.0	-28.8	-25.8[b]	-28.5	-26.2	-23.2[b]
LMoBr$_2$ + THF → **cis-LMoBr$_2$(THF)**	-29.5	-27.2	-23.9[b]	-26.0	-23.7	-20.4[b]
2 **LMoBr$_2$** → **[LMoBr$_2$]$_2$**	-44.8	-43.4	-32.0	-38.6	-37.2	-25.8
2 trans-**LMoBr$_2$(THF)** → **[LMoBr$_2$]$_2$** + 2 THF	17.2	14.1	19.5[b]	18.2	15.2	20.6[b]
LMoBr + **LMoBr$_3$** → [**LMoBr$_2$**]$_2$	-28.6	-27.0	-16.8	-27.6	-26.0	-15.8
LMoBr(THF)•THF + **LMoBr$_3$** → **[LMoBr$_2$]$_2$** + 2 THF	-5.3	-8.0	-0.6[b]	-14.9	-17.6	-10.2[b]

[a] Values after scaling translational and rotational entropies.

[b] Values including statistical correction for concentration of THF solvent.

S5.5. Thermodynamics of addition of CO to *cis*-LMoBr(CO)$_2$

Three distorted pentagonal-bipyramidal isomers (P = P^{i}Pr$_2$)
(M06 energies from gas phase calculations)

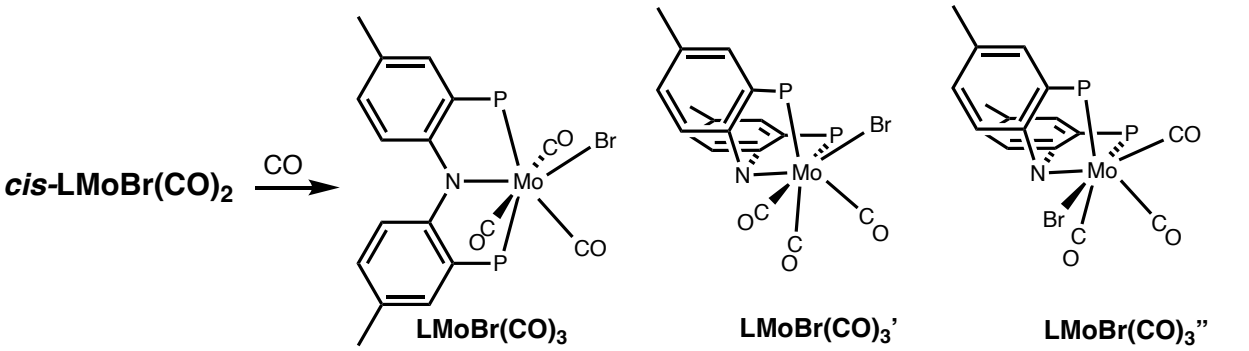

LMoBr(CO)$_3$
CO, CO-apical
(but not equivalent)
ΔE_{gas} = -15.8 kcal/mol

LMoBr(CO)$_3$'
CO, P^{i}Pr$_2$-apical
ΔE_{gas} = -4.7 kcal/mol

LMoBr(CO)$_3$"
Br, P^{i}Pr$_2$-apical
ΔE_{gas} = 8.2 kcal/mol

Gas-phase thermodynamics of **LMoBr(CO)$_3$** isomers at the M06/6-311g**/SDD(Mo,Br) level of theory

Solution-phase thermodynamics (in kcal/mol)

		M06D3			B3LYP-D3BJ		
Species	**Spin state**	ΔE	ΔH	ΔG[a]	ΔE	ΔH	ΔG[a]
LMoBr(CO)$_3$	Singlet	-16.5	-14.8	-3.5	-12.6	-10.7	0.6

[a] Values after scaling translational and rotational entropies.

S5.6. NBO Analysis

Natural bonding orbital (NBO) analysis of the quadruply-bonded dimer was performed using the Gaussian NBO Version 3.1 program[S28] interfaced with Gaussian 16 (revision A03). NBO population analysis was performed on the density obtained in the SMD continuum solvation model with THF solvent using the M06 global hybrid exchange-correlation functional[S14] with the Ahlrichs def2-tzvp basis set[S24,S25] on main group atoms and the def2-qzvp basis set[S26] on Mo. NBO analysis was obtained using the "pop=(nboread,savenbos)" keywords in the route card. The resultant NBOs were contained in the checkpoint (.chk) file, and all other relevant information was contained in the output (.log) file. The .chk file was converted to a formatted checkpoint (.fchk) file using the formchk utility included with Gaussian 16. The IQMol (v3.1.5) program was subsequently used to visualize NBOs contained in the .fchk file with an isovalue of 0.1000 a_0^3. In Figure 4, red and blue denote positive and negative phases respectively. The orthographic camera view was used to generate the images.

VI. References

(S1) L. Fan, B. M. Foxman and O. V. Ozerov, *Organometallics,* 2004, **23**, 326-328. DOI: 10.1021/om034151x.

(S2) A preprint of work describing N_2 splitting using **LMoBr$_3$** has been deposited on *ChemRxiv*: S. Mandal, S. Malakar, R. N. Allen, A. Tyryshkin, T. J. Emge, F. Hasanayn and A. S. Goldman, *ChemRxiv* 2025. doi: 10.26434/chemrxiv-2025-40qzq

(S3) D. F. Evans, *J. Chem. Soc.*, 1959, 2003-2005, doi: 10.1039/JR9590002003.

(S4) S. K. Sur, *J. Mag. Res.)*, 1989, **82**, 169-173, doi: 10.1016/0022-2364(89)90178-9.

(S5) G. M. Sheldrick, 1996. SADABS and TWINABS. University of Göttingen, Germany.

(S6) G. Sheldrick, *Acta Cryst., C* 2015, **71**, 3-8. doi: 10.1107/S2053229614024218

(S7) G. Sheldrick, *Acta Cryst., A* 2015, **71**, 3-8. doi: 10.1107/S2053273314026370

(S8) Bruker (2017). APEX3. Bruker AXS Inc., Madison, Wisconsin, USA

(S9) Bruker (2001). SHELXTL, XPREP, XP. Bruker AXS Inc., Madison, Wisconsin, USA.

(S10) C. R. Groom and F. H. Allen, *Angew. Chem., Intl. Ed.* 2014, **53**, 662-671. doi: 10.1002/anie.201306438

(S11) C. F. Macrae, P. R. Edgington, P. McCabe, E. Pidcock, G. P. Shields, R. Taylor, M. Towler and J. van de Streek, *J. Appl. Cryst.* 2006, **39**, 453-457. doi: 10.1107/S002188980600731X

(S12) M. J. Frisch, G. W. Trucks, H. B. Schlegel, G. E. Scuseria, M. A. Robb, J. R. Cheeseman, G. Scalmani, V. Barone, G. A. Petersson, H. Nakatsuji, X. Li, M. Caricato, A. V. Marenich, J. Bloino, B. G. Janesko, R. Gomperts, B. Mennucci, H. P. Hratchian, J. V. Ortiz, A. F. Izmaylov, J. L. Sonnenberg, Williams, F. Ding, F. Lipparini, F. Egidi, J. Goings, B. Peng, A. Petrone, T. Henderson, D. Ranasinghe, V. G. Zakrzewski, J. Gao, N. Rega, G. Zheng, W. Liang, M. Hada, M. Ehara, K. Toyota, R. Fukuda, J. Hasegawa, M. Ishida, T. Nakajima, Y. Honda, O. Kitao, H. Nakai, T. Vreven, K. Throssell, J. A. Montgomery Jr., J. E. Peralta, F. Ogliaro, M. J. Bearpark, J. J. Heyd, E. N. Brothers, K. N. Kudin, V. N. Staroverov, T. A. Keith, R. Kobayashi, J. Normand, K. Raghavachari, A. P. Rendell, J. C. Burant, S. S. Iyengar, J. Tomasi, M. Cossi, J. M. Millam, M. Klene, C. Adamo, R. Cammi, J. W. Ochterski, R. L. Martin, K. Morokuma, O. Farkas, J. B. Foresman and D. J. Fox, *Gaussian 16 Rev. A.03*; Wallingford, CT, 2016.

(S13) H.S. Yu, X. He, S.L. Li and D. G. Truhlar, *Chem. Sci.* 2016, **7**, 5032-5051, DOI: 10.1039/C6SC00705H.

(S14) Y. Zhao and D. G. Truhlar, *Theor. Chem. Acc.*, 2008, **120**, 215-241.

(S15) P. C. Hariharan and J. A. Pople, *Theo. Chim. Acta* 1973, **28**, 213-222. DOI: 10.1007/BF00533485.

(S16) M. S.Gordon, J. S. Binkley, J. A. Pople, W. J. Pietro and W. J. Hehre, *J. Am. Chem. Soc.* 1982, **104**, 2797-2803. DOI: 10.1021/ja00374a017.

(S17) M. M. Francl, W. J. Pietro, W. J. Hehre, J. S. Binkley, M. S. Gordon, D. J. DeFrees and J. A. Pople, *J. Chem. Phys.* 1982, **77**, 3654-3665. DOI: 10.1063/1.444267.

(S18) W. J. Hehre, R. Ditchfield and J. A. Pople, *J. Chem. Phys.* 1972, **56**, 2257-2261. DOI: 10.1063/1.1677527.

(S19) D. Andrae, U. Häußermann, M. Dolg, H. Stoll, H. Preuß, *Theo. Chim. Acta,* 1990, **77**, 123-141. DOI: 10.1007/BF01114537.

(S20) S. Grimme, J. Antony, S. Ehrlich and H. Krieg, *J. Chem. Phys.*, 2010, **132** 154104. DOI: 10.1063/1.3382344

(S21) A. D. Becke, *J. Chem. Phys.*, 1993, **98**, 5648-5652.

(S22) S. Grimme, S. Ehrlich and L. Goerigk, *J. Comp. Chem.* 2011, **32**, 1456-65. DOI: 10.1002/jcc.21759

(S23) C. J. Cramer, *Essentials of Computational Chemistry: Theories and Models, 2nd Edition*, Wiley, 2004.

(S24) A. Schäfer, C. Huber and R. Ahlrichs, *J. Chem. Phys.*, 1994, **100**, 5829-5835.

(S25) F. Weigend and R. Ahlrichs, *Phys. Chem. Chem. Phys.*, 2005, **7**, 3297-3305.

(S26) F. Weigend, F. Furche and R. Ahlrichs, *J. Chem. Phys.*, 2003, **119**, 12753-12762.

(S27) T. D. Lohrey, A. Q. Cusumano, W. A. Goddard, III and B. M. Stoltz, *ACS Catal.*, 2021, **11**, 10208-10222.

(S28) NBO Version 3.1, E. D. Glendening, A. E. Reed, J. E. Carpenter, and F. Weinhold.